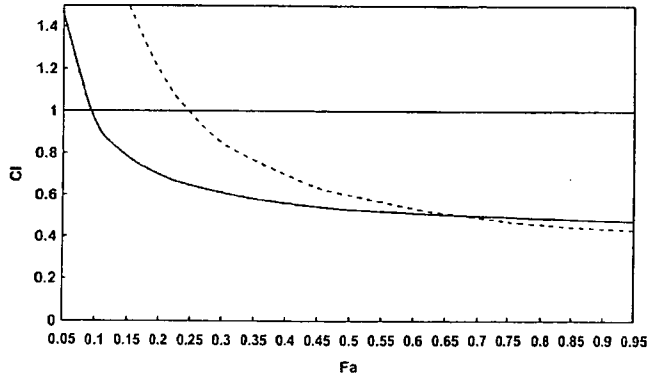

Fig. 6. Computer generated presentation of combination index (CI) with respect to the fraction affected (Fa) for the inhibition of FluV A/H1N1 multiplication in MDCK cells. Combination of PM-523 and ribavirin at ratio of 1:16 (—) and 1:4 (———) were analyzed under mutually nonexclusive assumptions.

Table 5
Cytotoxicity of PM-523 and ribavirin did not increase by their combined use

Concentration (μM)		
PM-523	Ribavirin	Percent viability of cells [a]
100	0	81.1 ± 2.9
200	0	89.3 ± 5.8
400	0	85.2 ± 3.5
0	100	107.2 ± 1.7
0	200	104.8 ± 3.8
0	400	102.8 ± 4.1
100	100	81.4 ± 3.8
100	400	66.8 ± 3.6
200	200	85.4 ± 3.8
400	100	79.2 ± 6.5
400	400	65.5 ± 9.3

[a] Viability of cells was determined by MTT method. Viability of the cells which were not treated with compounds was estimated as 100%.

indicated effect is additive. When the CI is >1, antagonism is indicated.

Combination effect was examined with combinations of PM-523 and ribavirin at 1:16 (———) and at 1:4 (———). As shown in Fig. 6, the CI values were always less than 1 when the fraction affected was determined to be between 0.25 (EC_{25}) and 0.95 (EC_{95}).

The cytotoxicity of PM-523, ribavirin and their combinations were examined by the trypan blue exclusion method. As shown in Table 5, a combination of 400 μM each of PM-523 and ribavirin exhibited a slightly increased cytotoxicity compared with that of the compounds used individually at 400 μM. However, the combination did not increase the cytotoxicity potently and 50% inhibition of cell viability was not obtained at any combination.

PM-523 and ribavirin exhibited a synergistic therapeutic effect in mice infected with FluV A (H1N1/PR8). One hundred percent of the control mice which were infected with 10 LD_{50} of the FluV A and not treated with the compounds died on the 9th day following infection. The infected mice were treated with aerosols of PM-523 and ribavirin either singly or in combination every 12 hours for 4 days. Compounds were prepared in PBS (pH 7.2) at concentrations from 1.2 to 4.8 mM for PM-

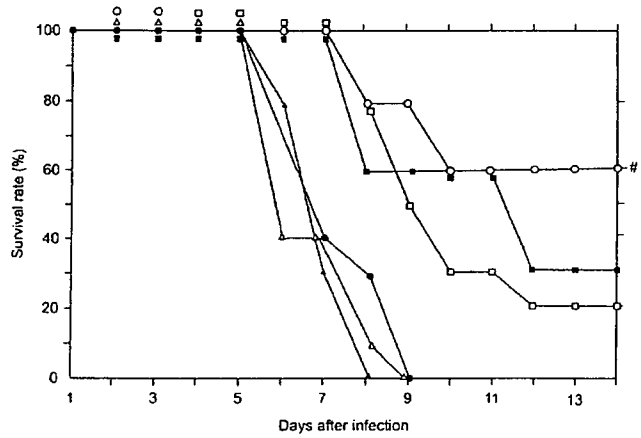

Fig. 7. Therapeutic effects of aerosol treatment of FluV A-infected mice with PM-523 and ribavirin. Mice were infected with virus (1.6×10^4 $TCID_{50}$) intranasally, and were exposed to aerosol of the compound solutions at the indicated conditions for 2 hours. The mice were exposed to the compounds every 12 hours for 4 days starting at 8 hours after virus inoculation. •, untreated control; ▲, ribavirin at 40 mM; ■, ribavirin at 80 mM; Δ, PM-523 at 2.4 mM; □, PM-523 at 4.8 mM; ○, PM-523 at 2.4 mM plus ribavirin at 40 mM. #, a level of significance of $P < 0.001$ against 40 mM ribabirin and 2.4 mM PM-523. $P < 0.01$ against 4.8 mM PM-523, $P < 0.05$ against 80 mM ribavirin.

523 and 40–240 mM for ribavirin. The infected mice were placed in a chamber separately and exposed to the compounds by using a continuous aerosol generator. In this experiment, the dose of the compound given to the mice was expressed in terms of the concentration of the compound in the stock solution. On the 9th day when all of the control (untreated) mice died, half and 60% of the mice treated with 4.8 mM PM-523 and 80 mM ribavirin survived. The EC_{50}s of PM-523 and ribavirin on the 9th day of infection were calculated as 4.8 and 70 mM, respectively. When 2.4 mM PM-523 (0.5 EC_{50}) and 40 mM ribavirin (0.57 EC_{50}) were combined and used to treat the infected mice, 80% of the mice survived to the 9th day following infection. At the end of the experiment (14 days after the infection, as indicated in Fig. 7), survival was found for 60%, 30% and 20% of the infected mice in the groups in which a combination of 2.4 mM PM-523 and 40 mM ribavirin, 80 mM ribabirin alone, and 4.8 mM PM-523 alone were used. Thus the survival rate for mice treated with a combination of PM-523 and ribavirin at a ratio of 1:16 was significantly higher than for mice in groups which received a single treatment of twice the dose of PM-523 (4.8 mM) and ribavirin (80 mM) throughout the experiment (Fig. 7). The lungs of infected and untreated mice and mice treated with 2.4 mM PM-523 or 40 mM ribavirin alone became swollen and reddened due to congestion. On the other hand, the lungs of infected mice treated with a combination of 2.4 mM PM-523 and 40 mM ribavirin remained a more normal grayish white and were not congested (data not shown). The viral titer in the lungs of the infected mice was determined for four groups of mice every 24 hours after infection. As shown in Fig. 8, the viral titers in infected mouse lungs increased to $10^{5.4}$ $TCID_{50}$/g at 48 hors following infection and decreased to $10^{3.5}$ and $10^{3.2}$ $TCID_{50}$/g at 72 and

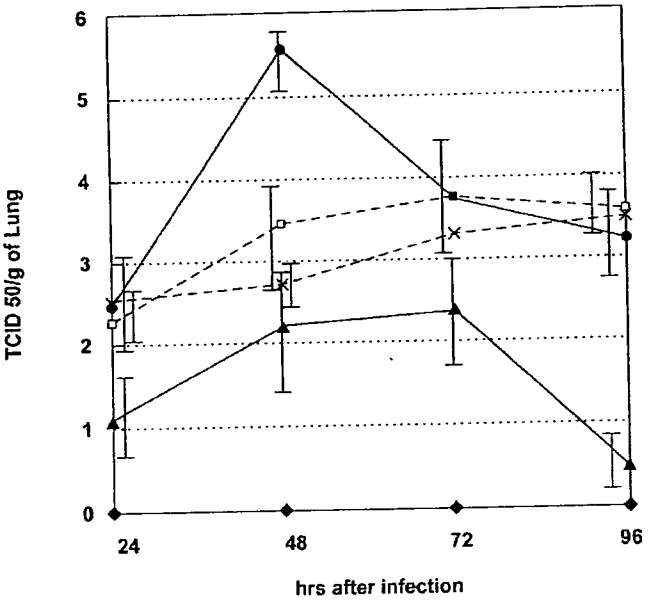

Fig. 8. Virus titer in lungs of FluV A infected mice. Mice were infected in the same manner as described in the legend to Fig. 7. Three mice in each group were sacrificed at the indicated times, and their lungs were homogenized separately, diluted and centrifuged. Infective virus in the supernatant was titrated using MDCK cells and $TCID_{50}$ was determined. ♦, noninfected control mice; ●, infected and untreated mice; □, mice treated with 2.4 mM PM-523; ×, mice treated with 40 mM ribavirin; and ▲, mice treated with 2.4 mM PM-523 plus 40 mM ribavirin.

96 hours, respectively. The viral titers in the lungs of infected mice which were treated with a combination of PM-523 (2.4 mM) and ribavirin (40 mM) were consistently lower than those in the lungs of control mice or those treated with the compounds individually (Fig. 8) [5].

6. Broad spectrum anti-RNA virus activities of titanium and vanadium substituted polyoxotungstates

Several workers have reported anti RNA virus POM activity. Ikeda et al. [6] reported that JM2820 had broad spectrum antiviral activity including activity against the ortho- and para-myxoviruses, herpesviruses and retroviruses (HIV-1 and 2). JM-2820 is the same compound as HS-106, which we previously reported to have a broad spectrum anti-myxovirus activity (Table 1). Barnard et al. [7] reported anti-RSV activities of several polyoxotungstates and among them HS-106 and certain germanium- or zirconium-containing polyoxotungstates (JM-2926 and JM-2919, respectively) exhibited the most potent and selective anti-RSV activity. HS-106 and JM-2926 have double Keggin structures and JM-2919 has a Barrel structure. They commented that silicon, germanium and niobium centered double Keggin structures yielded antiviral activity. Huffman et al. [8] also reported anti-FluV (FluV A and B) activities of germanium or silicon containing polyoxotungstates. They singled out especially JM-2925 (a germanium containing double Keggin-type polyoxotungstate) and JM-2919 as potent and selective anti-FluV compounds. Liu et al. [9] (a Chinese chemist group) synthesized a heteropoly blue from a Keggin-type polyoxotungstate $\{Ce_2H[BW_{11}Mn(H_2O)O_{39}]\}$. This compound, designated HPB-2, exhibited a potent therapeutic effect against FluV infection in mice when given either orally or intraperitoneally.

These reports prompted us to identify broad spectrum anti-RNA virus POM and use them for the therapy of acute viral respiratory infections. We examined seven titanium or vanadium substituted polyoxotungstates (all have Keggin or Keggin

Table 6
Chemical structure of polyoxotungstates

Compound [a]	Chemical formula	Species of structure
PM-43	$K_5[SiVW_{11}O_{40}]$	Keggin
PM-47	$K_7[BVW_{11}O_{40}]$	Keggin
PM-518	$[Et_2NH_2]_7[PTi_2W_{10}O_{40}]$	Keggin
PM-520	$[Pri_2NH_2]_5[PTiW_{11}O_{40}]$	Keggin
PM-523	$[PriNH_3]_6[PTi_2W_{10}O_{38}(O_2)_2]H_2O$	Keggin
PM-1001 [b]	$K_{10}Na[(VO)_3(SbW_9O_{33})_2]26H_2O$	Keggin sandwich
PM-1002 [b]	$K_{11}H[(VO)_3(SbW_9O_{33})_2]27H_2O$	Keggin sandwich

[a] PM-518, PM-520, PM-523 possess a Ti atom and PM-43, PM-47, PM-1001 possess a V atom.
[b] PM-001 and PM-1002 have the same core structure of $(VO)_3(SiW_9O_{33})_2$; however, the V3 of PM-1001 consists of two V^{IV} and one V^{V} while that of PM-1002 consists of three V^{IV}.

Table 7
Broad spectrum anti-RNA virus activities of Ti and V substituted polyoxotungstates

Compound	EC_{50} (μM) [a]					
	DFV [b]	FluV A [b]	RSV [b]	PfluV 2 [b]	CDV [c]	HIV-1 [b]
PM-43	10.7 ± 6.7	8.4 ± 6.5	1.6 [d]	> 100	7.5 ± 1.0	0.3 ± 0.12
PM-47	10.5 ± 6.9	11.5 ± 0.6	29.0 [d]	67.1 [d]	6.0 ± 0.6	0.03 ± 0.01
PM-518	36.8 ± 3.0	62 ± 27	26.5 [d]	53 ± 39	> 50	2.0 ± 0.8
PM-520	11.7 ± 7.1	45 ± 26	0.74 ± 0.6	23 ± 2.4	7.4 ± 0.4	2.0 ± 0.5
PM-523	> 61.5	5.6 ± 2.0	1.3 ± 0.5	2.5 ± 1.3	7.3 ± 1.1	0.3 ± 0.1
PM-1001	0.45 ± 0..1	1.75 ± 1.6	< 0.16	1.1 ± 0.9	5.7 ± 0.5	0.14 ± 0.17
PM-1002	2.0 ± 1.4	4.0 ± 1.7	0.75 ± 0.05	0.75 ± 0.05	2.8 ± 1.0	0.03 ± 0.01
Ribavirin	> 100	5.0 ± 2.8	3.9 ± 3.1	14.0 ± 4.8	74 ± 35	Nd [e]

[a] Average values for three to seven independent experiments.
[b] EC_{50} was determined by MTT method.
[c] EC_{50} was determined by plaque reduction method.
[d] Average of two experiments.
[e] Not determined.

sandwich structures, Table 6) for Dengue virus, PfluV 2, canine distemper virus (CDV, a paramyxovirus related to measles virus) and human immunodeficiency virus (HIV) 1.

All of the compounds exhibited broad spectrum anti-RNA virus activity except that PM-43, PM-518 and PM-523 did not have antiviral activities against PfluV 2, CDV and DFV, respectively. All compounds demonstrated potent anti-HIV activity. Among them two vanadium-substituted double Keggin polyoxotungstates, PM-1001 and PM-1002, exhibited particularly potent and selective anti-HIV activities in vitro (Table 7). When anti-HIV activities were examined with a MAGI test using HeLa CD4/LTR-β-Gal cells, the EC_{50}s of the compounds were 10 and 18 nM, and their selectivity indices exceeded 10,000 and 5000, respectively. PM-1001 and 1002 showed their anti-HIV activities at an early stage of the infection (probably at the adsorption stage) and also inhibited syncytium formation between MOLT-4 cells (uninfected cells) and MOLT-4/IIIb cells (infected cells). In order to analyze the target molecule with which PM-1001 interacts during the adsorption/penetration process, we examined the inhibitory effect of PM-523 against the binding of mouse antibodies to CD4, CXCR4 (monoclonal) and gp-120 (polyclonal) to the target molecules. PM-1001 inhibited the binding of anti-gp120 antibody to gp-120 but did not inhibit the binding of the anti-CD4 and anti-CRCX4 antibodies to their target molecules. Probably PM-1001 is inhibitory for the interaction of gp120 with its receptors, but the binding site is gp-120 (not CD4) [10]. A similar result on the POM anti-HIV mechanism of action has been reported by Witvrouw et al. [11] using Dowson and double Dawson structured polyoxotungstates. However, they suggested also the blocking of gp-120 binding to the CD4 molecule by a covering of the receptor site by the compounds.

7. Anticoronavirus activities of polyoxometalates

Severe acute respiratory syndrome (SARS) first emerged in late 2002 in Guangdong province, southern China, and then spread to the neighboring countries and, eventually, around the world. Eight thousand or more people have been judged to be probable cases of infection, and about 750 patients lost

Table 8
Antiviral activities of polyoxometalates against coronaviruses

	EC_{50}(μM) [a]			SI [c]		
	TGEV [b]	FIPV [c]	SARS-V [d]	TGEV	FIPV	SARS-V
PM-504	1.4 ± 0.5	0.4 ± 0.3	3.5 ± 2.4	> 12.8	> 46.7	> 14.3
PM-518	2.1 ± 1.1	> 32.9	> 50	> 15.6	□1.0	< 1.0
PM-520	1.4 ± 1.3	0.76 ± 0.5	4.9 ± 1.4	> 20.4	>38.5	> 10.3
PM-523	2.5 ± 0.6	> 32.0	> 50	> 32.0	□1.0	< 1.0
PM-802	0.5 ± 0.5	0.03 ± 0.01	> 50	4.9	97.2	< 1.0
PM-803	0.34 ± 0.3	> 21.0	Nd	55.3	□1.0	–
PM-1001	0.14 ± 0.1	0.2 ± 0.1	0.7 ± 0.4	83.6	84.4	> 70.4
PM-1002	0.6 ± 0.4	Nd	0.25 ± 0.07	18.6	–	> 400
PM-1201	0.2 ± 0.14	> 9.0	Nd	> 100	□1.0	–
PM-1207	1.9 ± 1.4	0.09 ± 0.04	0.9 ± 0.24	> 9.3	35.2	> 54.3
PM-1208	2.0 ± 1.8	> 3.6	2.7 ± 0.6	> 8.1	□1.0	> 18.4
PM-1210	1.6 ± 1.1	0.74 ± 0.4	0.76 ± 0.3	> 6.6	> 14.3	>65.8
PM-1213	1.7 ± 1.0	> 10.5	0.47 ± 0.14	> 18.2	□1.0	106.4

[a] EC_{50} and CC_{50} were determined by the average of three independent experiments.
[b] Transmissible gastroenteritis virus of swine.
[c] Feline infectious peritonitis virus.
[d] SARS coronavirus.
[e] Selectivity index. SIs were calculated by CC_{50}/EC_{50} in which the CC_{50}s were determined by cytotoxicities for CPK cells (TGEV), for fcwf-4 cells (FIPV) and for Vero cells (SARS-V), respectively. The SIs greater than 30 are indicated in bold face.

Table 9
Chemical formula of polyoxotungstates

Compound	Chemical formula	Color [a]	Species
PM-504	$K_7H_5[Ge_2Ti_6W_{18}O_{77}]16H_2O$	White	Keggin Dimer
PM-518	$[Et_2NH_2]_7[PTi_2W_{10}O_{40}]$	White	Keggin
PM-520	$[Pri_2NH_2]_5[PTiW_{11}O_{40}]$	White	Keggin
PM-523	$[PriNH_3]_6H[PTi_2W_{10}O_{38}(O_2)_2]2H_2O$	Orange	Keggin
PM-802	$Na_7H_9\{Eu_3O(OH)_3(H_2O)_3\}_2Al_2(Nb_6O_{19})_5\}$ $47H_2O$	White	Lindqvist Trigonal
PM-803	$(NBu_4)_4(PriNH_3)$ $[PTi_2W_{10}O_{38}(O_2)_2]2H_2O$	Yellow	Keggin
PM-1001	$K_{10}Na[(VO)_3(SbW_9O_{33})_2]26H_2O$	Black	Keggin Sandwich
PM-1207	$K_{12}[(VO)_3(AsW_9O_{33})_2]12H_2O$	Dark brown	Keggin Sandwich
PM-1208	$K_{12}[(VO)_3(BiW_9O_{33})_2]29H_2O$	Black	Keggin Sandwich
PM-1210	$[NH_4]_{12}H(BiW_9O_{33})_3Bi_6(OH)_3$ $(H_2O)_3V_4H_{10}]25H_2O$	Brown	Keggin Trigonal
PM-1213	$K_{12}[(VO)_3(PW_9O_{34})_2]nH_2O$	Dark grey	Keggin Sandwich

[a] Color of powder.

their lives. The etiological agent was originally defined as a novel corona virus and later designated the SARS coronavirus.

Coronaviruses are widely distributed among avian and mammalian species and commonly cause infections [12]. The replication cycle of the coronavirus in permissive cells is common and for the adsorption to cellular membrane receptors the N-terminal portion of the viral spike glycoprotein of the envelope is used [13]. Since POMs have been proven to inhibit the adsorption of several of the enveloped RNA viruses we examined nine titanium or vanadium containing polyoxotungstates and one heteropolyoxometalate in which tungsten was substituted with niobium (PM-802 in Table 9). Three coronaviruses which were shown to be pathogenic to mammals were used. These viruses were transmissible gastroenteritis virus of swine (TGEV), feline infectious peritonitis virus (FIPV) and SARS coronavirus (SARS-V), respectively.

As shown in Table 8 all of the POMs exhibited anti-TGEV activities. For SARS-V, the vanadium-substituted Keggin sandwich type POMs displayed activity. For FIPV there is no apparent relationship between the structure and the antiviral activity. Over all, PM-1001 and PM-1207, which are vanadium-substituted Keggin sandwich type polyoxotungstates, exerted the most potent and selective anti-coronavirus activities (Table 8).

8. Conclusion

We previously reported that PM-1001 possesses broad spectrum anti-RNA virus activities including activity against FluV A, RSV, PfluV 2 and so on. This compound also displays potent and selective anti-SARS-V activity in vitro. Although, as yet there are no reports of POMs in clinical use, most of the in vitro and some of the in vivo experiments have shown these compounds to be potent and broad spectrum in terms of their antiviral activities against acute respiratory disease viruses. Since the clinical diagnosis of respiratory virus infection is difficult, and laboratory confirmation is excessively time consuming, broad spectrum antiviral compounds such as ribavirin, interferons and POMs are promising as initial treatments of undetermined respiratory viral diseases. Further work will elucidate which of these drugs, and which combinations of these drugs, should be added to the clinical pharmacopeia.

Acknowledgements

I would like to thank Prof. Tatsuo Suzutani for the strong supports for the preparations of data on anti-coronavirus activity of POM, figures and tables.

References

[1] Mori S, Watanabe W, Shigeta S. A colorimetric LDH assay for the titration of infectivity and the evaluation of antiviral activity against ortho- and paramyxoviruses. Tohoku J Exp Med 1995;177:315–25.
[2] Shigeta S, Mori S, Watanabe J, Baba M, Khenkin AM, Hill CL, et al. In vitro anti-myxovirus and anti-human immunodeficiency virus activities of polyoxometalates. Antivir Chem Chemother 1995;6:114–22.
[3] Shigeta S, Mori S, Watanabe J, Yamase T, Schinazi RF. *In-vitro* anti myxovirus activity and mechanism of anti-influenzavirus activity of polyoxometalates PM-504 and PM-523. Antivir Chem Chemother 1996; 7:346–52.
[4] Shigeta S. Targets of anti-influenza chemotherapy other than neuraminidase and proton pomp. Antivir Chem Chemother 2001;12(Supple 1) 179–88.
[5] Shigeta S, Mori S, Watanabe J, Soeda S, Takahashi K, Yamase T. Synergistic anti-influenza virus A (H1N1) activities of PM-523 (polyoxometalate) and ribavirin in vitro and in vivo. Antimicrob Agents Chemother 1997;:1423–7.
[6] Ikeda S, Neyts J, Yamamoto N, Murrer B, Theobald B, Bossard G, et al. In vitro activity of a novel series of polyoxosilicotungstates against human myxo- herpes- and retroviruses. Antivir Chem Chemother 1993; 4:253–62.
[7] Barnard DL, Hill CL, Gage T, Matheson JE, Huffman JH, Sidwell RW, et al. Potent inhibition of respiratory syncytial virus by polyoxometalates of several structural classes. Antivir Res 1997;34:27–37.
[8] Huffman JH, Sidwell RW, Barnard DL, Morrison A, Otto MJ, Hill CL, et al. Influenza virus-inhibitory effects of a series of germanium- and silicon centered polyoxometalates. Antivir Chem Chemother 1997;8:75–83.
[9] Liu J, Mei W, Li Y, Wang E, Ji L, Tao P. Antiviral activity of mixed-valence rare earth borotugstate heteropoly blues against influenza virus in mice. Antivir Chem Chemother 2000;11:367–72.
[10] Shigeta S, Mori S, Kodama E, Kodama J, Takahashi K, Yamase T. Broad spectrum activities of titamium and vanadium substituted polyoxotaungstates. Antivir Res 2003;58:265–71.
[11] Witvrouw M, Weigold H, Pannecouque C, Schols D, De Clercq E, Holana G. Potent anti-HIV (Type 1 and Type 2) activity of polyoxometalates: Structure–activity relationship and mechanism of action. J Med Chem 2000;43:778–83.
[12] Shigeta S, Yamase T. Current status of anti-SARS agents. Antivir Chem Chemother 2005;16:23–32.
[13] Lai MMC, Holmes KV. Coronaviridae: the viruses and their replication. In Fields's Virology, 4th ed. Philadelphia: Lippincott-Williams & Wilkins, 1163–85.

Int. J. Cancer: **119**, 823–830 (2006)

Human T-cell leukemia virus type-I Tax induces expression of interleukin-6 receptor (IL-6R): Shedding of soluble IL-6R and activation of STAT3 signaling

Sankichi Horiuchi[1], Norio Yamamoto[1], Md. Zahidunnabi Dewan[1,2], Yoshiaki Takahashi[3], Atsuya Yamashita[4], Tsutomu Yoshida[5], Mari A. Nowell[6], Peter J. Richards[6], Simon A. Jones[6] and Naoki Yamamoto[1,2]*

[1]*Department of Molecular Virology, Tokyo Medical and Dental University, Tokyo, Japan*
[2]*AIDS Research Center, National Institute of Infectious Diseases, Tokyo, Japan*
[3]*Department of Infectious Disease and Immunology, Okinawa Asia Research Centre of Medical science, University of the Ryukyus, Okinawa, Japan*
[4]*Department of Microbiology, Interdisciplinary Graduate School of Medicine and Engineering University of Yamanashi, Yamanashi, Japan*
[5]*Biophenix Co., Ltd., Ube Yamaguchi, Japan*
[6]*Medical Biochemistry and Immunology, School of Medicine, Cardiff University, Cardiff, UK*

Human T-cell leukemia virus type-I (HTLV-I) encodes for the viral protein Tax, which is known to significantly disrupt transcriptional control of cytokines, cytokine receptors and other immuno-modulatory proteins in T cells. Specific dysregulation of these factors can alter the course and pathogenesis of infection. Soluble interleukin-6 receptor (sIL-6R) was shown to circulate at elevated levels in HTLV-I-infected patients, and high expressions of IL-6R and sIL-6R by HTLV-I-infected T cells were clinically and experimentally associated with Tax activity. To examine roles of Tax in expression of the IL-6R gene, the JPX-9 cell line was used, which is derived from Jurkat cell line expressing Tax cDNA. Over-expression of Tax enhanced IL-6R expression but not in Tax mutant JPX-9/M cell line. The clinical relevance of these observations was further demonstrated by ELISA using sera obtained from HTLV-I-infected patients. Our results revealed that sIL-6R levels were apparently elevated in HAM/TSP patients who were expressing Tax in their cells, while ATL patients' cells barely expressed Tax. HTLV-I-infected T-cell lines stimulated by IL-6/sIL-6R showed gp130-mediated STAT3 activity. IL-6/sIL-6R enhanced proliferation of HTLV-I-infected T cells in association with activation of STAT3. Consequently, Tax-mediated regulations of IL-6R and sIL-6R observed in HTLV-I-associated disorders may contribute to proliferation of HTLV-I-infected T cells through activation of inducible STAT3, and ultimately affect malignant growth and transformation of T cells by HTLV-I.

Key words: HTLV-I; IL-6R; STAT3

Human T-cell leukemia virus type-I (HTLV-I) is the etiological agent of adult T-cell leukemia (ATL),[1,2] and is associated with a series of disease conditions including HTLV-I-associated myelopathy/tropical spastic paraparesis (HAM/TSP),[3] arthropathy,[4] and HTLV-I-associated uveitis (HU).[5] Although HTLV-I can infect various cell types,[6,7] it predominantly infects T lymphocytes, thereby promoting perpetual cellular proliferation and transformation of human T cells.

A key component in the control of these responses is expression of the HTLV-I-encoded transcriptional regulator Tax, which immortalizes cells *in vitro*, and initiates tumor progression *in vivo*.[8,9] Tax has been shown to activate the expression of a number of cellular genes through several distinct transcription factors such as NF-κB/Rel, AP-1 and serum response factor.[10,11] Cellular genes induced by Tax include cytokines/chemokines (IL-1α, IL-6, IL-8, TNF-β, MCP-1, GM-CSF and G-CSF), their receptors (IL-2Rα and IL-15R), cell adhesion molecules (OX40), matrix metalloproteinases (MMP-9), apoptosis inhibitors (Bcl-xL) and G1-cyclins (cyclin D1 and cyclin D2).[10,12–14] Transcriptional activation of cellular genes by Tax is thought to contribute to deregulated proliferation of HTLV-I-infected cells.

Interleukin-6 (IL-6) is a multifunctional cytokine that acts on different target cells to induce a variety of biological responses, such as B cell differentiation,[15] acute phase response[16] and proliferation of hemopoietic cells.[17] IL-6 activates the JAK/STAT pathway through two membrane proteins: the ligand-binding receptor IL-6R[18] and the signal transducing protein gp130.[19] Central to regulation of IL-6 mediated responses is the presence of soluble IL-6 receptor (sIL-6R), which forms a ligand–receptor complex allowing IL-6 responsiveness in cell types not expressing IL-6R.[20,21] This IL-6/sIL-6R complex can activate cells that do not normally respond to IL-6 through interaction with gp130. Although sIL-6R is released into body fluids of normal individuals, high levels of sIL-6R are associated with various diseases[22–26] by promoting a number of biological responses.[25] In the present study, we show that Tax is capable of inducing IL-6R gene transcription in T cells and is involved in promoting proteolytic (shedding) cleavage of cognate IL-6R. Regulation of these events may help explain the perpetual growth of HTLV-I-infected cells.

Materials and methods

Cell lines and cell growth assay

MT-2, MT-4, TY8-3/MT-2,[27] TY8-3/TCL-Kan,[27] HUT-102 and SLB-1 are HTLV-I-infected transformed T-cell lines. ILT-8M2[28] was obtained from a HTLV-I-infected carrier. TL-Oml, ED-40515 and C5MJ are HTLV-I-infected leukemic T-cell lines. TY8-3,[27] Jurkat and MOLT-4 are HTLV-I-negative T-cell lines. JPX-9[29] and JPX-9/M[30] lines are derivatives of Jurkat cells and possess stably integrated Tax or a mutant Tax under the control of a metallothionein promoter, respectively. The mutant Tax gene was developed by inserting one amino acid (arginine) between amino acids no. 62 and 63. For expression of Tax, cells were cultured in the presence of $CdCl_2$ (10 μM) at 37°C for 0–3 days. Cells were cultured in RPMI-1640 medium with 10% fetal bovine serum (FBS), 100 U/ml penicillin and 100 μg/ml streptomycin at 37°C and 5% CO_2. To examine cell growth by stimulation with IL-6/sIL-6R, HUT-102, MT-4 and TY8-3/MT-2, cells

Abbreviations: ATL, adult T-cell leukemia; EMSA, electrophoretic mobility-shift assay; FACS, fluorescence-activated cell sorter; HAM/TSP, HTLV-I associated myelopathy/tropical spastic paraparesis; HTLV-I, human T-cell leukemia/lymphotropic virus type-I; PBMC, peripheral blood mononuclear cells; sIL-6R, soluble interleukin 6 receptor; STAT3, signal transducer/activator of transcription.

Grant sponsor: Ministry of Health, Labor and Welfare, Ministry of Education, Culture, Sports, Science and Technology, Japanese Health Sciences Foundation and Wellcome Trust Biomedical.

*Correspondence to: Department of Molecular Virology, Tokyo Medical and Dental University, 1-5-45 Yushima, Bunkyo-ku, Tokyo 113-8519, Japan. Fax: +81-3-5803-0124. E-mail: yamamoto.mmb@tmd.ac.jp

Received 6 November 2005; Accepted after revision 18 January 2006
DOI 10.1002/ijc.21918
Published online 23 March 2006 in Wiley InterScience (www.interscience.wiley.com).

were washed twice with RPMI-1640 medium without FBS. Then, 10^5 cells/ml were cultured in RPMI-1640 without FBS in the presence or absence of IL-6 (50 ng/ml, Genzyme Techno, No. 2206), sIL-6R (100 ng/ml) and rabbit anti-human-IL-6 polyclonal antibody (500 ng/ml, IM-R109, Diaclone) at 37°C for 0–4 days. Numbers of viable cells were counted by the trypan blue staining method.

Patients and sera

Sera of 24 patients with ATL or of 13 patients with HAM/TSP who were outpatients or admitted to hospital from November 2002 to May 2003 were studied. Sera of 10 healthy control individuals were also used.

Polymerase chain reaction

RNA was extracted from cells using Isogen reagent (Nippon Gene CO., LTD). PCR was performed for 30 cycles of denaturation at 91°C for 1 min, followed by annealing at 62°C for 1 min and polymerization at 72°C for 1 min. Oligonucleotide primers used for PCR amplification of IL-6R were as follows: forward, 5′-ACGCCTTGGACAGAATCCAG-3′ and reverse, 5′TGGCTC GAGGTATTGTCAGA-3′.[31] Primers used for PCR amplification of β-actin were as follows: forward, 5′-CCTTCTACAATGAGCTGCGTG-3 and reverse, 5′-ACAGCCTGGATAGCAACG TACA-3′.

Flow cytometric analysis

Expression of IL-6R was analyzed by indirect flow cytometry with a FACS Calibur cell sorter (Becton-Dickinson). Cells (5×10^6) were washed with PBS, treated with 70% methanol for 5 min and washed with PBS. After incubation with 5 μg/ml mouse anti-human IL-6R antibody (MCA822, Serotec) for 1 hr on ice, cells were washed with cold PBS, and incubated for 1 hr with 5 μg/ml goat anti-mouse IgG FITC-conjugated antibody (A106FU, Cappel). Following a final wash, fluorescence intensity was measured from 10,000 gated events.

Western blot

Cells (1×10^7) were incubated for 30 min in 0.3 ml low salt lysis buffer [10 mM Tris-HCl (pH 8.0), 140 mM NaCl, 3 mM $MgCl_2$, 1 mM PMSF, 0.5% NP40, 1 mM DTT] and then centrifuged for 20 min at 15,000 rpm. Equal amounts (10 or 25 μg) of proteins were used for 10% SDS-PAGE and were transferred to PVDF membranes by electroblotting. Blots were incubated with monoclonal anti-Tax antibody (MI-73) and were subsequently incubated with anti-mouse Ig conjugated with horseradish-peroxidase (A206PS, American Qualex Antibodies). Antibody binding was visualized using the ECL western blotting detection system (Amersham).

ELISA for cell-associated cognate IL-6R and PC-sIL-6R

Cells were suspended in fresh medium at a concentration of 4×10^5 cells /ml and cultured for 72 hr. Then, 2×10^7 cells were washed twice with PBS and suspended in 0.5 ml cold low salt lysis buffer. After incubation for 30 min at 4°C, cell lysates were centrifuged at 15,000 rpm for 20 min and stored at −70°C. Concentration of cells associated with IL-6R was measured using an ELISA kit (DR600, R & D systems, Minneapolis). sIL-6R was measured in culture supernatants using a commercial ELISA kit. Concentrations of differentially spliced IL-6R mRNA (DS-sIL-6R) were quantified using a monoclonal antibody (mAb-2F3) as capture antibody.[26] Amount of proteolytic cleavage of cognate IL-6R (PC-sIL-6R) was predicted by subtracting the concentration of DS-sIL-6R from that of total sIL-6R.

Construction of expression vectors encoding PC-sIL-6R

cDNA coding for PC-sIL-6R was constructed using PCR technology, with template DNA and pGEM-T (IL-6R).[26] The oligonucleotide primer pair 6R5F (5′-CGCGGATCCGCGCATCATCATCATCATCATCTGGCCCCAAGGCGCTGCCCTGCG-3′) and 6R3R (5′-GGAATTCCCTACACTGGGAGGCTTGTCGCATTTGC-3′) was used for PCR. The obtained constructs carried a BamHI restriction enzyme site, 6 His tags at the N-terminus and an EcoRI site at the C-terminus. PCR products were cloned into baculovirus transfer vectors pMel Bac A (Invitrogen).

Production of recombinant PC-sIL-6R

Recombinant baculoviruses were produced by homologous recombination, as indicated in the Bac-N-Blue Transfection Kit manual (450432, Invitrogen). A single recombinant baculovirus encoding PC-sIL-6R was isolated using a plaque assay and was amplified by infecting Sf-9 cells. High Five cells (B855-02, Invitrogen) were infected with recombinant baculoviruses obtained from Sf-9 cells. Proteins were purified using Ni-NTA agarose, according to the manual (30210, Qiagen). Samples were analyzed by silver staining or Western blot analysis. Protein purity was high (data not shown).

Stimulation of cells and preparation of nuclear extracts

Cells (2.5×10^7) were washed twice with cold PBS, resuspended in 1 ml serum-free RPMI medium containing 0.5% BSA and incubated with IL-6 (50 ng/ml) and PC-sIL-6R (100 ng/ml) for 30 min at 37°C. Cells were washed twice with cold PBS and resuspended in hypotonic buffer [20 mM HEPES (pH 7.8), 10 mM KCl, 0.15 mM EGTA and 0.15 mM EDTA], supplemented with protease inhibitors (1 mM PMSF, 1 μg/ml leupeptin and 1 μg/ml aprotinin). After 15-min incubation at 4°C, NP40 was added to reach a concentration of 1%, and the cells were vortexed for 20 sec. After centrifugation, nuclear pellets were briefly washed with isotonic buffer [20 mM HEPES (pH 7.8), 100 mM NaCl, 0.1 mM EDTA and 25% glycerol] and resuspended in extraction buffer [20 mM HEPES (pH 7.8), 400 mM NaCl, 0.1 mM EDTA, 25% glycerol, 1 mM DTT and 1 mM PMSF]. After 30-min incubation at 4°C with occasional agitations, supernatants were recovered by centrifugation at 15,000 rpm for 2 min, and protein concentration was determined using the Bradford method.

Electrophoresis mobility shift assay (EMSA)

Nuclear extracts (5 μg proteins) were added to binding buffer for STAT3 probe [10 mM HEPES (pH 7.8), 1 mM EDTA, 5 mM $MgCl_2$, 4% glycerol, 5 mM DTT, 0.7 mM PMSF, 0.1 μg/ml poly d (I-C) and 1 mg/ml BSA] or to binding buffer for transcription factor OCT-1 probe [10 mM Tris-HCl (pH 7.5), 50 mM NaCl, 1 mM EDTA, 1 mM DTT, 4% glycerol, 0.1 μg /ml poly d (I-C) and 1 mg/ml BSA]. In addition, γ-^{32}P-labeled STAT3 probes (5′-CGGGAGGGATTTACGGGAAATGCTA-3′) or γ-^{32}P-labeled OCT-1 probes (5′-TGTCGAATGCAAATCACTAGAA-3′) were added to the mixtures and incubated for 15 min at room temperature. Samples were run on a 5% polyacrylamide gel in 0.5× Tris-borate EDTA. Gels were dried and analyzed by autoradiography. For competition studies, 50 times excess unlabeled STAT3 or NF-κB probes were included in the reaction.[32]

Results

Expression of IL-6R in HTLV-I-infected T cells

To determine whether induction of IL-6R gene transcription in T cells correlated with HTLV-I infection, RT-PCR was performed on HTLV-I-infected and -uninfected human T-cell lines. A 398 bp PCR product corresponding to IL-6R was detected in HTLV-I-infected T-cell lines except for ED-40515 (Fig. 1*a*, lanes 5–10) but in none of the uninfected lines. Indeed, FACS analysis of all HTLV-I-infected T-cell lines showed a marked induction of IL-6R expression (Fig. 1*b*), whilst IL-6R was not detected in HLTV-I-negative lines MOLT-4 and Jurkat (data not shown). To substantiate HTLV-I control of IL-6R expression, studies were performed using a parental TY8-3 cell line and TY8-3 cells infected with HTLV-I (TY8-3/MT-2 and TY8-3/TCL-Kan). Cognate IL-6R expression was significantly enhanced in TY8-3/MT-2 and TY8-3/TCL-Kan cell lines, while IL-6R expression in the parental line was negative (Figs. 1*a* and 1*b*). Increased IL-6R expression was further confirmed using an ELISA-based approach to monitor IL-

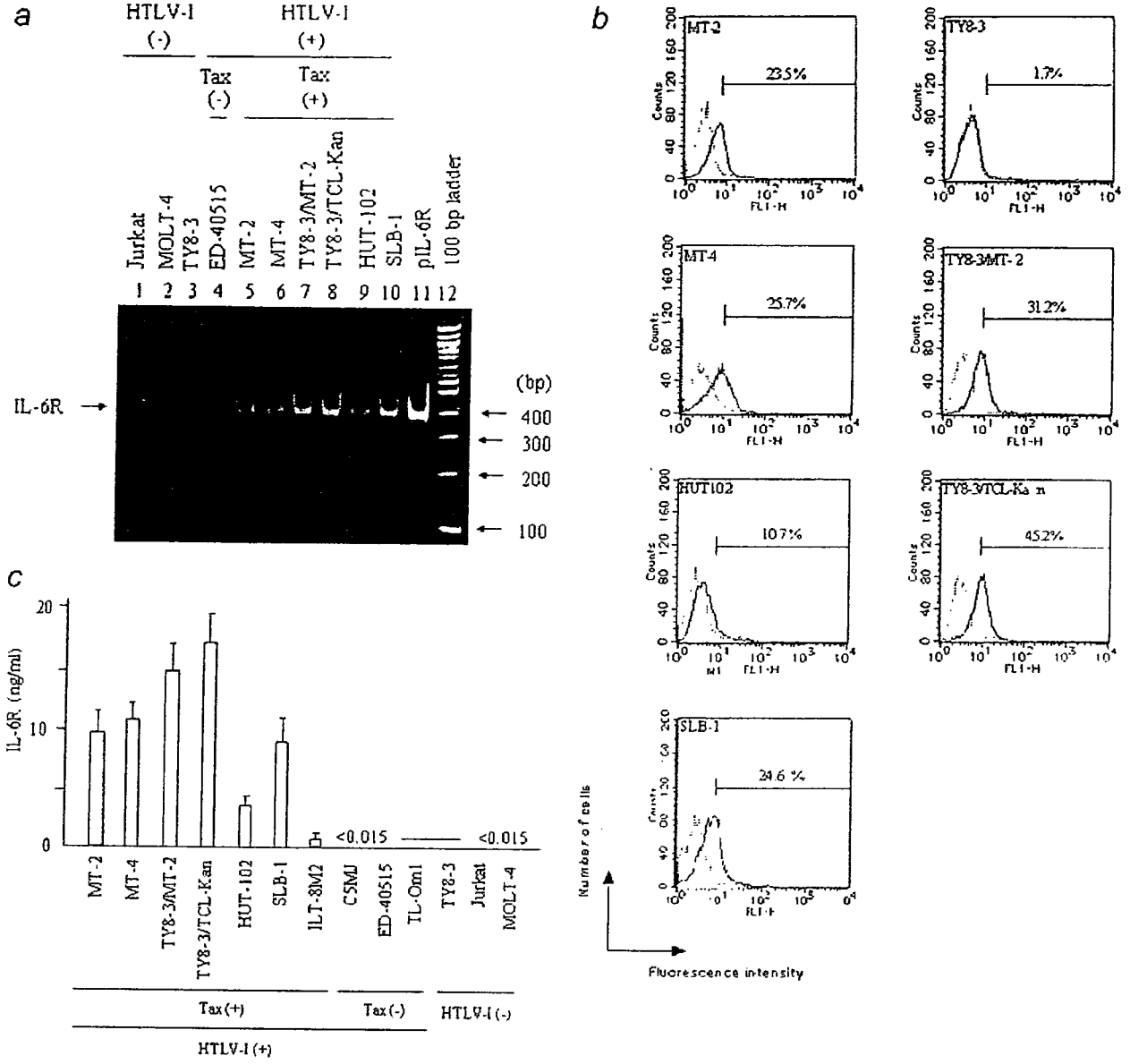

FIGURE 1 – Expression of IL-6R in HTLV-I-infected human T cells. (*a*) Detection of IL-6R by RT-PCR in human T-cell lines. mRNA was subjected to PCR using specific forward and reverse primers. PCR products were analyzed by SDS-PAGE. Lane 11: Plasmids carrying IL-6R DNA were used as positive control. Molecular size of the plasmid is 398 bp. (*b*) Surface expression of IL-6R in T-cell lines. Cells were treated with anti-human IL-6R antibody for 1 hr on ice. Subsequently, they were treated with goat anti-mouse IgG FITC-conjugated antibody for 1 hr on ice. Dotted line histograms show background staining with isotype control antibodies, and solid line histograms show specific staining. (*c*) Measurement of IL-6R using cell lysates of T-cell lines with or without HTLV-I. Cells were lysed with low salt lysis buffer, and after centrifugation, the resultant supernatants were used for ELISA. Data are representative examples of three reproducible experiments.

6R levels within cell lysates. As shown in Figure 1*c*, there was a correlation between HLTV-I infection and IL-6R expression, with no evidence of IL-6R expression in the HTLV-I-negative cell lines TY8-3, Jurkat and MOLT-4.

Tax induces expression of the IL-6R gene

The transcriptional activator Tax has previously been reported to account for induction of several host cell genes during HTLV-I infection, and Tax regulation of IL-2, IL-2R, IL-6 and IL-15R occurs through NF-κB.[10,33–36] To test whether Tax promoted expression of cognate IL-6R, Tax expression was monitored by Western blot in various HTLV-I-infected and -uninfected T-cell lines (Fig. 2). All Tax-positive cell lines showed IL-6R expression, while none of the Tax-negative cells expressed IL-6R. Indeed, the parental TY8-3 cell line showed no Tax or IL-6R expression, but the HTLV-I-infected cell lines TY8-3/MT-2 and TY8-3/TCL-Kan expressed both Tax and IL-6R (Figs. 1*c* and 2). However, in TY8-3/TCL-kan and HU-T102 cell lines, degree of Tax expression did not necessarily correlate with levels of IL-6R detected. This lack of direct correlation may be attributable to the use of different cell lines.

To establish a firm correlation and functional link between Tax and IL-6R expression, experiments were performed using a JPX-9

cell line transfected with $CdCl_2$-inducible Tax constructs.[29] As shown in Figures 3*a* and 3*b*, addition of $CdCl_2$ to the culture medium of transfected JPX-9 cells resulted in an increase in Tax protein and a concomitant increase in IL-6R expression occurring within 24 h of Tax induction. This increase in IL-6R expression was due to Tax activity, since a functionally inactive form of Tax (JPX-9/M) failed to promote IL-6R expression (Fig. 3*b*, lanes 6–9). These results indicated that Tax was involved in constitutive expression of the IL-6R gene. Although transcriptional mechanisms for induction of IL-6R remain unclear, Tax induction directly coincided with up-regulation of IL-6R. Taken together, these results suggested that the levels of Tax expression, at least in part, correlated with induction of IL-6R expression.

Elevated level of sIL-6R in culture supernatants of Tax-positive HTLV-I-infected T cells

Since previous studies have established that HTLV-I infection resulted in elevated sIL-6R,[26] experiments tested whether the observed increases in cognate IL-6R coincided with increases in sIL-6R. Soluble IL-6R levels were therefore quantified in supernatants from HTLV-I-infected T-cell lines. To distinguish between the two isoforms of sIL-6R, two ELISA approaches were utilized to delineate sIL-6R production *via* PC-sIL-6R or DS-sIL-6R.[37–39] Although a close association between HTLV-I infection and sIL-6R production was evident, DS-sIL-6R release could not be detected in any of the cell lines tested (data not shown), suggesting that HTLV-I predominantly affected release of PC-sIL-6R. As shown in Figure 4*a*, sIL-6R production was evident in almost all Tax-positive cell lines and was very high in TY8-3/TCL-kan cells but not in the isogenic parental T-cell line TY8-3. In contrast, PC-sIL-6R was not produced in the Tax-negative T-cell lines TL-Om1, ED-40515 and C5MJ. ILT-8M2 produced less than 15 pg/ml PC-sIL-6R. This may be related to lower level of expression of cognate IL-6R in ILT-8M2 cells. Thus, in induction of IL-6R gene expression by Tax, Tax activity may be associated with increased IL-6R shedding, although the shedding mechanism is not clear.

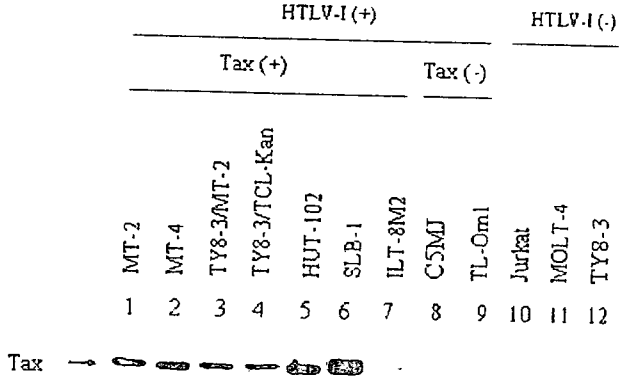

FIGURE 2 Expression of Tax protein in HTLV-I-infected or -uninfected T cells. Cell lysates (10 μg protein) were prepared from the indicated cell lines and Tax in each lysate was detected by Western blot analysis using an anti-Tax antibody (MI-73).

Detection of high levels of PC-sIL-6R in sera of HTLV-I-infected patients

We next examined secretion of PC-sIL-6R in sera of HTLV-I-infected patients. Sera obtained from ATL or HAM/TSP patients were analyzed using ELISA. Higher levels of PC-sIL-6R were found in HAM patients (mean = 73.4 ng/ml) compared with healthy persons (mean = 19.1 ng/ml) (Fig. 4*b*). Moderate levels of PC-sIL-6R were detected in ATL patients (mean = 34.5 ng/ml) with a significant probability ($p = 0.016$). Lower levels of DS-sIL-6R were found in healthy persons (mean = 1.6 ng/ml), ATL (mean = 4.3 ng/ml) and HAM patients (mean = 4.1 ng/ml), respectively.

STAT3 signaling by IL-6/sL-6R in HTLV-I-infected T cells

HTLV-I induces transformation of human $CD4^+$ T cells, an event that correlates with acquisition of constitutive phosphorylation of Janus kinases (JAK), signal transducers and activators of transcription (STAT) proteins. However, it is unclear whether these proteins are activated by the IL-6/IL-6R/gp130 complex. Since the above results suggested that Tax induced IL-6R, we next examined STAT3 activation of HTLV-I-infected cells after stimulation with IL-6/PC-sIL-6R complexes. As shown in Figure 5*a*, EMSA analysis of STAT3 activation revealed that the HTLV-I-infected T-cell lines TY8-3/MT-2, TY8-3/TCL-Kan and MT-2 possessed constitutively activated STAT1 and STAT3. However, activation of these STAT factors remained unaffected in these cell lines following stimulation with IL-6 and PC-sIL-6R. Antibodies against IL-6 and IL-6R did not abolish constitutive STAT3 activation of TY8-3/MT-2 and TY8-3/TCL-Kan cell lines (data not shown), suggesting that constitutive activation may not be dependent on IL-6 stimulation in these cell lines. In fact, HTLV-I-infected T-cell lines expressed high levels of various types of cytokines such as IL-2, IL-6, IL-7, IL-9 and IL-15.[34–36,40] Therefore, it is possible that some cells depend on IL-6/IL-6R to activate STAT3, while others do not.

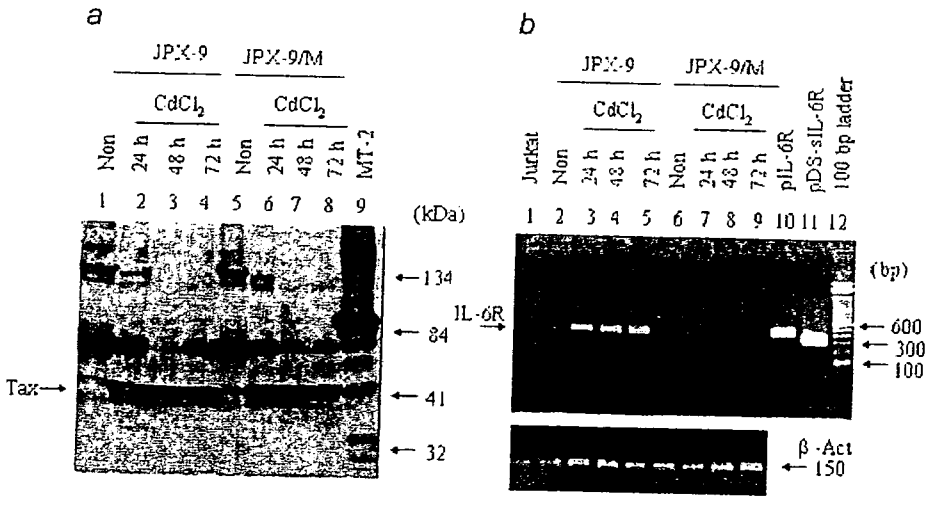

FIGURE 3 – Correlation of IL-6R up-regulation with HTLV-I Tax synthesis. (*a*) Expression of Tax in JPX-9 cells (Western blot). Cells were cultured in the presence of $CdCl_2$ (10 μM)) for 0–72 h. Cell lysates (25 μg protein) were prepared and Tax was detected by Western blot analysis. (*b*) Expression of IL-6R in JPX-9 cells (RT-PCR). JPX-9 and JPX-9/M were cultured in the presence of $CdCl_2$ (10 μM)) for 0–72 hr. RNA was extracted from these cells, and expression of IL-6R was analyzed by RT-PCR. Amplified fragments were analyzed by 2% agarose gel. Lanes 10 and 11: Plasmids carrying IL-6R DNA or DS-sIL-6R DNA were used as positive controls. Molecular sizes of these plasmids are 304 and 398 bp, respectively.

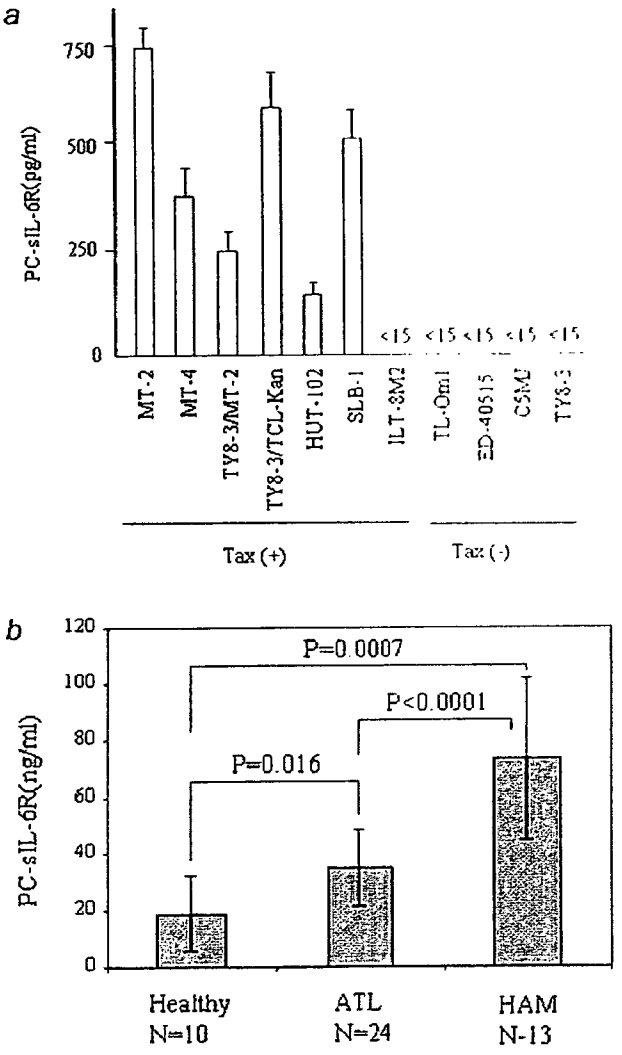

FIGURE 4 - Secretions of PC-sIL-6R and IL-6 into HTLV-I-infected T cells. (*a*) Release of PC-sIL-6R from HTLV-I-infected or -uninfected T-cell lines. PC-sIL-6R concentrations were measured in culture supernatants of mature cells, using a commercially available ELISA kit. Data are representative examples of three reproducible experiments. (*b*) Serum levels of PC-sIL-6R in a healthy person, ATL and HAM/TSP patients determined by ELISA. Serum levels represent an average of three independent measurements.

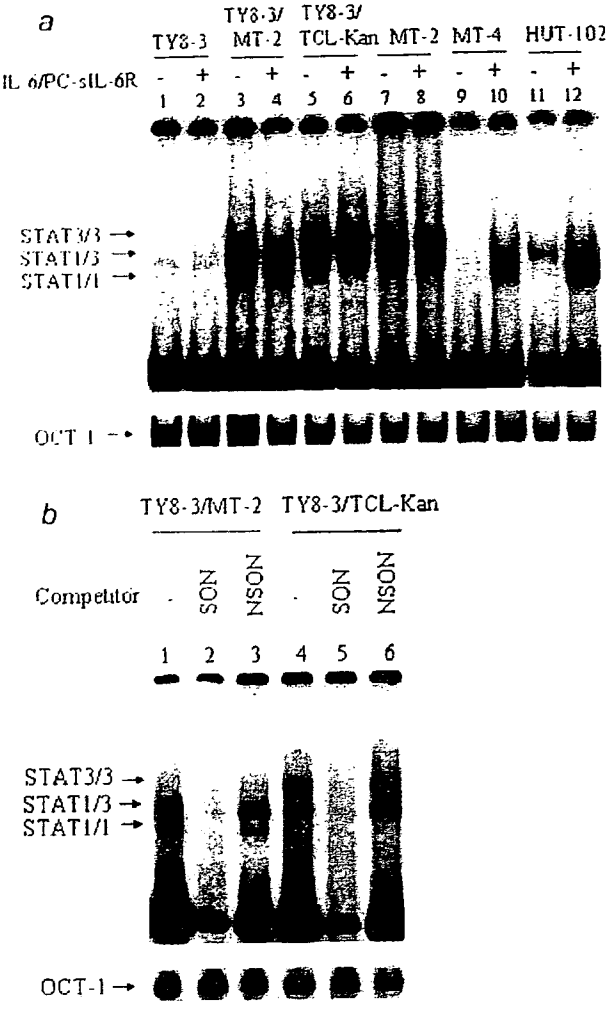

FIGURE 5 - Activation of STAT3 in HTLV-I-infected T cells. (*a*) Nuclear extracts from cell lines stimulated with IL-6/PC-sIL-6R. Nuclear extracts were analyzed in an EMSA using radiolabeled STAT3 oligonucleotides. DNA-protein complexes were separated by electrophoresis. STAT3 is constitutively activated in HTLV-I-infected cell lines but some cell lines respond to stimulation by IL-6/PC-sIL-6R. Arrows show positions of STAT3 and STAT1 homodimers and heterodimers. OCT-1 served as internal control for each sample. (*b*) Competition experiments of STAT3. For competition studies, 50-fold excess of unlabeled probes was included in the binding reaction. Competition experiments were carried out in the absence or presence of unlabeled specific oligonucleotides (SON, STAT3) or unlabeled nonspecific oligonucleotides (NSON, NF-κB).[32] DNA-protein complexes were separated by electrophoresis.

In contrast, STAT3 was not constitutively activated in MT-4 but weakly activated in HUT-102. These cell lines were stimulated with IL-6/PC-sIL-6R and were found to promote STAT3 activity (Fig. 5*a*, lanes 9–12). Activation of these signaling components was elicited through PC-sIL-6R-mediated signaling, since blockade of IL-6 events with an anti-human IL-6R antibody prevented activations of STAT1 and STAT3 (data not shown). DNA-protein complexes of MT-4 and HUT-102 migrated faster than complexes observed in TY8-3/TCL-Kan or MT-2 cells, suggesting that activation of STAT3 variants such as STAT3-β occurred.[40] Stimulation of ED-40515 cell line with IL-6/PC-sIL-6R was also found to promote STAT3 activity (data not shown). Stimulation of TY8-3 (Fig. 5*a*, lanes 1–2), MOLT-4 and Jurkat T-cell lines with IL-6/PC-sIL-6R showed no evidence of STAT3 activation (data not shown for MOLT-4 and Jurkat). To confirm specific DNA binding of STAT3 components, competition assays were performed with nuclear extracts from TY8-3/MT-2 and TY8-3/TCL-kan cells and with unlabeled specific STAT1/3 oligonucleotides, resulting in disappearance of the three bands (Fig. 5*b*, lanes 2 and 5). On the other hand, incubation of nuclear extracts with unlabeled nonspecific oligonucleotides (NF-κB) resulted in no disappearance of the three bands (Fig. 5*b*, lanes 3 and 6). Taken together, these experiments suggested that IL-6 and sIL-6R activated STAT3 protein in HTLV-I-infected T-cell lines.

Proliferation of HTLV-I-infected cell lines by stimulation with IL-6/PC-sIL-6R

STAT belongs to a family of transcriptional factors mediating various cytokine signaling.[41]

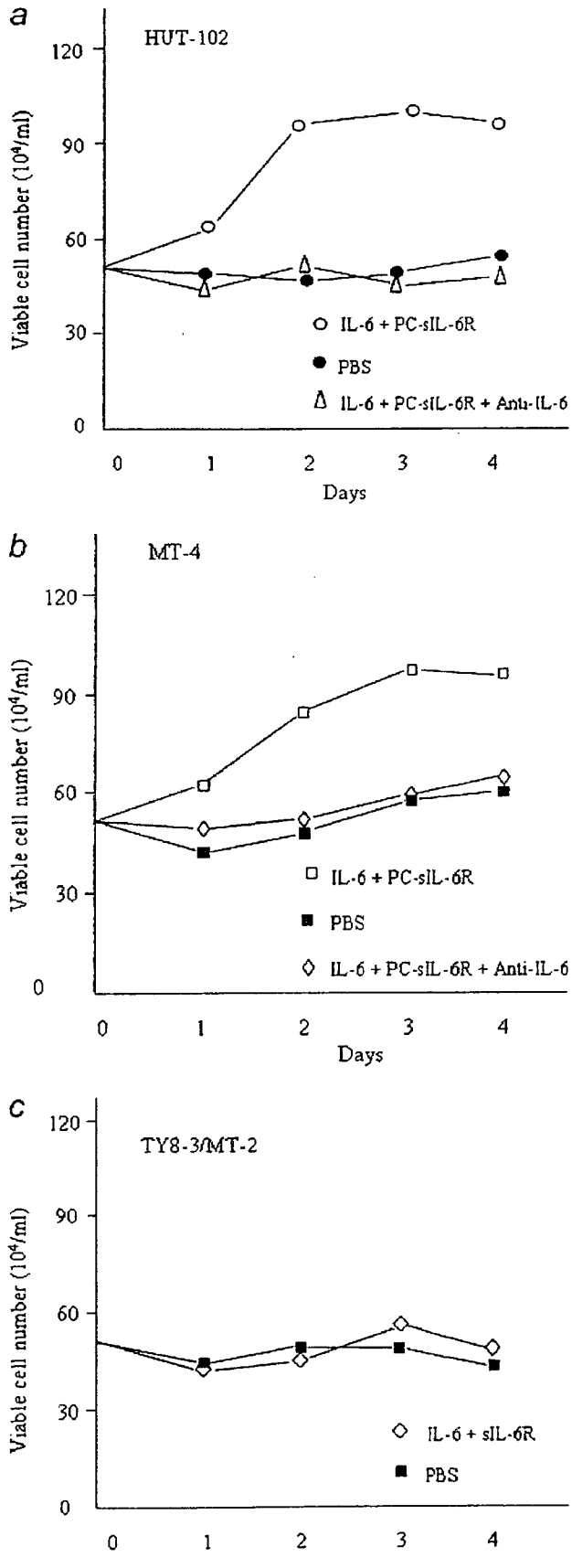

DNA binding activity of STAT3 was induced by IL-6/PC-sIL-6R in HUT-102 and MT-4 cell lines but not in TY8-3/MT-2 cells (Fig. 5*a*). Therefore, these cell lines were useful to examine roles of STAT3 in IL-6/PC-sIL-6R induction. Consequently, IL-6-mediated proliferation assays were performed under serum-free conditions. IL-6/sIL-6R enhanced proliferation of HUT-102 and MT-4 cells (Figs. 6*a* and 6b) but not that of TY8-3/MT-2 (Fig. 6*c*). IL-6/PC-sIL-6R-induced proliferation of HUT-102 and MT-4 cells was specifically blocked by anti-human IL-6 antibody. Thus, IL-6/PC-sIL-6R-induced proliferation in these two cell lines correlated with DNA binding activity of STAT3 protein. Therefore, PC-sIL-6R may play a role in immortalization of HTLV-I-infected T cells.

Discussion

Elevated levels of sIL-6R in serum have been associated with the pathogenesis of several disease states such as HIV-I infection, HAM/TSP and rheumatoid arthritis.[22-24,26] This implies that sIL-6R production increases as part of an inflammatory response. However, little is known on factors that might regulate expression of IL-6R or sIL-6R generation. In the present report, we investigated expression of IL-6R in T lymphocytes and the release of its soluble receptor from HTLV-I-infected T-cell lines. In particular, HTLV-I infection of T cells led to induction of IL-6R gene transcription and increased release of soluble IL-6R. Regulation of these events appears to be dependent on activity of the viral transcriptional regulator Tax.

In this study, we showed a clear association between HTLV-I-infection and IL-6R expression on T cells by RT-PCR and FACS analysis, and measured IL-6R proteins by ELISA. Characteristics of HTLV-I-infected T-cell lines are listed in Table I. Since HTLV-I encodes the transcriptional regulator Tax, which is a transcriptional activator for viral genes and a number of cellular genes,[33,42] we investigated roles of Tax in expression of IL-6R. Using a JPX-9 cell line, we found that induction of Tax expression resulted in enhanced IL-6R expression. These results indicated that Tax was capable of constitutive expression of IL-6R. In accordance with this observation, Tax-negative leukemic cell lines ED-40515, TL-Om1 and C5MJ derived from ATL patients were negative for IL-6R, though they possessed HTLV-I genome (Table I).

We also examined production of soluble IL-6R in culture medium of HTLV-I-infected T-cell lines. Since two distinct isoforms of IL-6R (PC-sIL-6R and DS-sIL-6R) have been previously identified, we measured each type using specific antibodies coating plates. PC-sIL-6R was detected in TY8-3/MT-2 and TY8-3/TCL-Kan cells but not in the HTLV-I uninfected TY8-3 cell line. DS-sIL-6R was not detected in culture medium of any T-cell lines. Thus, these results clearly indicated that HTLV-I could only induce PC-sIL-6R but not DS-sIL-6R probably due to consequences of enhanced proteolytic shedding. Although we previously showed that DS-sIL-6R levels increased in serum of patients with ATL and HAM/TSP, increased release of DS-sIL-6R might be associated with a systemic response based on inflammation. Indeed, in HTLV-I-unrelated patients with elevated levels of antinuclear antibodies or α-fetoprotein, levels of DS-sIL-6R are also high compared with those of a healthy person.[26] We examined relationships between production of soluble IL-6R and Tax

FIGURE 6 -- Cell growth analysis of HUT-102 (*a*), MT-4 (*b*) and TY8-3/MT-2 (*c*) cells. Cells were washed with RPMI-1640 medium without FBS, and then cultured in RPMI-1640 without FBS, in the presence or absence of IL-6 and PC-sIL-6R. In the neutralization test, IL-6/PC-sIL-6R was preincubated with anti-human IL-6 antibody (IM-R109, Diaclone) for 60 min at room temperature and then added to HUT-102 or MT-4 cell lines for stimulation. Cell growth was measured by trypan blue staining. Representative data are shown among three reproducible independent experiments.

TABLE I – CHARACTERISTICS OF HTLV-I INFECTED T CELL LINES

Cell lines	Origin[1]	HTLV-I	Tax	IL-6R[2]	PC-sIL-6R[3]
HUT-102	IT	+	+	+	+
MT-4	IT	+	+	+	+
TYS-3/MT-2	IT	+	+	+	+
TY8-3/TCL-Kan	IT	+	+	+	+
MT-2	IT	+	+	+	+
SLB-1	IT	+	+	+	+
ILT-8MT	HC	+	+	+	
ED-40515	L	+			
TL-Oml	L	+			
C5MJ	L	+			
TY8-3	THY	–			
Jurkat	ALL				
MOLT-4	ALL	–			

+, positive; –, negative.
[1]IT, *in vitro* transformed T cell; HC, HTLV-I-carrier; L, leukemic T-cell; TYH, thymoma T-cell line; ALL, acute lymphocytic leukemia.–[2]Expression of IL-6R was detected by RT-PCR, FACS and ELISA. [3]Concentration of PC-sIL-6R was measured by ELISA

expression. PC-sIL-6R was produced at high levels in Tax-positive cell lines but not in Tax-negative cell lines. Thus, it is likely that Tax also induces PC-sIL-6R protein *in vivo*. This is supported by our observation that PC-sIL-6R protein was detected at higher levels in sera of HAM/TSP patients (Fig. 4*b*) in which Tax-positive cells were present in peripheral blood[13] compared with sera of healthy people or ATL patients, who are known to barely contain them. These results indicate that Tax enhances production of PC-sIL-6R in HTLV-I-infected T cells.

STAT belongs to a family of transcriptional factors mediating various cytokine signals.[41] In many human malignant cells and transformed cells, STAT3 is constitutively activated. The IL-6/sIL-6R complex can activate JAK/STAT signaling pathway, leading to oncogenesis, proliferation and survival.[44] HTLV-I-infected cell cultures become, with time, IL-2-independent and acquire a constitutive activation of JAK/STAT protein.[45] We examined STAT3 activation of HTLV-I-infected cells. In *in vitro* transformed cell lines such as MT-4 and HUT-102, STAT3 protein was not constitutively or weakly activated, respectively. In contrast, STAT3 was constitutively activated in TY8-3/MT-2, TY8-3/TCL-Kan and MT-2 cells (Fig. 5*a*). We also examined relationships between STAT3 activation and proliferation in HTLV-I- infected cells. Proliferation of HUT-102, MT-4 and TY8-3/MT-2 cells was examined using serum-free medium. IL-6/PC-sIL-6R stimulated proliferation of HUT-102 and MT-4 cells and was apparently associated with activation of STAT3 protein, whereas proliferation of TY8-3/MT-2 cells was not affected. Therefore, our finding that IL-6R was induced by Tax suggests that Tax might play a role in leukemogenesis *in vivo*, such as immortalization of HTLV-I-infected T cells.

Molecular mechanisms of ATL and HAM/TSP have not yet been elucidated. A characteristic feature of these diseases is infiltration of lymphocytes including virus-infected cells into affected tissues such as lymph nodes and the central nervous system, respectively. Recent studies have suggested that abnormal signal transduction in HTLV-I-infected T-cell lines[40,46,47] or cytokine overproduction were involved in diseases caused by HTLV-I.[48,49] Clinically, it is interesting to note that a high level of production of sIL-6R is associated with T cell abnormalities such as AIDS and HAM.[23,26] It is speculated that sIL-6R may play a role in a wide variety of both normal and abnormal biological reactions. Once bound to IL-6, the resulting IL-6/sIL-6R complex acts as an agonist that is capable of activating cells through gp130.[21] Several studies showed that IL-6/sIL-6R complex could induce proliferation of synovial fibroblastic cells.[50] Moreover, the IL-6/sIL-6R complex has been reported to regulate leukocyte recruitment and to promote proinflammatory stimulation of endothelial cells.[51,52] In particular, sIL-6R-mediated signaling directs transition between innate and acquired immune responses by suppressing neutrophil infiltration and promoting mononuclear leukocyte influx. This occurs through regulation of local inflammatory chemokine expression and cellular apoptotic events.[20,53] Such processes may be relevant to HTLV-I-related diseases, since these conditions are associated with increased lymphocyte infiltration. Indeed, IL-6 has been found to rescue T cells from entering apoptosis.[54–56] Consequently, enhanced expressions of IL-6, IL-6R and sIL-6R following HTLV-I infection may contribute to propagation of HTLV-I associated disorders.

This study is the first report to show that HTLV-I induces production of soluble IL-6R in T cells, and this induction is Tax-dependent. We speculate that HTLV-I modulates cellular signal transduction pathways leading to leukemic proliferation of virus-infected cells. Tax induces production of both IL-6[36] and soluble IL-6R (in this study). Thus, HTLV-I/Tax regulation of sIL-6R release could facilitate formation of agonistic IL-6/ sIL-6R complex and perpetuate the IL-6 response.

Acknowledgements

We thank Y. Inagaki for his technical assistance, and S. Yamaoka for providing anti-Tax antibodies. This work was supported in part by grants-in-aid from the Ministry of Health, Labor and Welfare, the Ministry of Education, Culture, Sports, Science and Technology of Japan; and the Japanese Health Sciences Foundation to S.H., and N.Y. and by grants from the Wellcome Trust Biomedical to S.A.J.

References

1. Hinuma Y, Nagata K, Hanaoka M, Nakai M, Matsumoto T, Kinoshita KI, Shirakawa S, Miyoshi I. Adult T-cell leukemia: antigen in an ATL cell line and detection of antibodies to the antigen in human sera. Proc Natl Acad Sci USA 1981;78:6476–80.
2. Poiesz BJ, Ruscetti FW, Gazdar AF, Bunn PA, Minna JD, Gallo RC. Detection and isolation of type C retrovirus particles from fresh and cultured lymphocytes of a patient with cutaneous T-cell lymphoma. Proc Natl Acad Sci USA 1980;77:7415–9.
3. Gessain A, Barin F, Vernant JC, Gout O, Maurs L, Calender A, The GD. Antibodies to human T-lymphotropic virus type-1 in patients with tropical spastic paraparesis. Lancet 1985;2:407–10.
4. Nishioka K, Maruyama I, Sato K, Kitajima I, Nakajima Y, Osame M. Chronic inflammatory arthropathy associated with HTLV-I. Lancet 1989;1:441.
5. Mochizuki M, Watanabe T, Yamaguchi K, Takatsuki K, Yoshimura K, Shirao M, Nakashima S, Mori S, Araki S, Miyata N. HTLV-I uveitis: a distinct clinical entity caused by HTLV-I. Jpn J Cancer Res 1992;83:236–9.
6. Green PL, Chen ISY. Human T-cell leukemia virus type 1 and 2. In: Knipe DM, Howley PM, eds. Fields virology. Philadelphia: Lippincott Williams and Wilkines, 2001. 1941–61.
7. Yamamoto N, Matsumoto T, Koyanagi Y, Tanaka Y, Hinuma Y. Unique cell lines harbouring both Epstein-Barr virus and adult T-cell leukaemia virus, established from leukaemia patients. Nature 1982; 299:367–9.
8. Akagi T, Ono H, Shimotohno K. Characterization of T cells immortalized by Tax1 of human T-cell leukemia virus type 1. Blood 1995;86: 4243–9.
9. Iwakura Y, Tosu M, Yoshida E, Takiguchi M, Sato K, Kitajima I, Nishioka K, Yamamoto K, Takeda T, Hatanaka M, Yamamoto H, Sekiguchi T. Induction of inflammatory arthropathy resembling rheumatoid arthritis in mice transgenic for HTLV-I. Science 1991;253: 1026–8.
10. Ballard DW, Bohnlein E, Lowenthal JW, Wano Y, Franza BR, Green WC. HTLV-I tax induces cellular proteins that activate the κB element in the IL-2 receptor α gene. Science 1988;241:1652–5.
11. Fujii M, Niki T, Mori T, Matsuda T, Matsui M, Nomura N, Seiki M. HTLV-I Tax induces expression of various immediate early serum responsive genes. Oncogene 1991;6:1023–9.
12. Huang Y, Ohtani K, Iwanaga R, Matsumura Y, Nakamura M. Direct trans-activation of the human cyclin D2 gene by the oncogene product Tax of human T-cell leukemia virus type I. Oncogene 2001;20:1094–102.

13. Mori N, Prager D. Transactivation of the interleukin-1α promoter by human T-cell leukemia virus type I and type II Tax proteins. Blood 1996;87:3410–7.
14. Mori N, Yamada Y, Ikeda S, Yamasaki Y, Tsukasaki K, Tanaka Y, Tomonaga M, Yamamoto N, Fujii M. Bay 11–7082 inhibits transcription factor NF-κB and induces apoptosis of HTLV-I-infected T-cell lines and primary adult T-cell leukemia cells. Blood 2002;100:1828–34.
15. Kishimoto T, Hirano T. Molecular regulation of B lymphocyte response. Annu Rev Immunol 1988;6:485–512.
16. Gauldie J, Richards C, Harnish D, Lansdorp P, Baumann H. Interferon β 2/B-cell stimulatory factor type 2 shares identity with monocyte-derived hepatocyte-stimulating factor and regulates the major acute phase protein response in liver cells. Proc Natl Acad Sci USA 1987;84:7251–5.
17. Ikebuchi K, Wong GG, Clark SC, Ihle JN, Hirai Y, Ogawa M. Interleukin 6 enhancement of interleukin 3-dependent proliferation of multipotential hemopoietic progenitors. Proc Natl Acad Sci USA 1987;84:9035–9.
18. Yamasaki K, Taga T, Hirata Y, Yawata H, Kawanishi Y, Seed B, Taniguchi T, Hirano T, Kishimoto T. Cloning and expression of the human interleukin-6 (BSF-2/IFN beta 2) receptor. Science 1988;241:825–8.
19. Taga T, Kawanishi Y, Hardy RR, Hirano T, Kishimoto T. Receptors for B cell stimulatory factor 2. Quantitation, specificity, distribution, and regulation of their expression. J Exp Med 1987;166:967–81.
20. Hurst S, Wilkinson T, Mcloughlin R, Jones SA, Horiuchi S, Yamamoto N, Rose-Jone S, Fuller G, Topley N, Jones S. IL-6 and its soluble receptor orchestrate a temporal switch in the pattern of leukocyte recruitment seen during acute inflammation. Immunity 2001;14:705–14.
21. Jones SA, Horiuchi S, Topley N, Yamamoto N, Fuller GM. The soluble interleukin 6 receptor: mechanisms of production and implications in disease. FASEB J 2001;15:43–58.
22. Desgeorges A, Gabay C, Silacci P, Novick D, Roux-Lombard P, Grau G, Dayer JM, Vischer T, Gueme PA. Concentrations and origins of soluble interleukin 6 recepter-α in serum and synovial fluid. J Rheumatol 1997;24:1510–6.
23. Honda M, Yamamoto S, Cheng M, Yasukawa K, Suzuki H, Saito T, Osugi Y, Tokunaga T, Kishimoto T. Human soluble IL-6 receptor: its detection and enhanced release by HIV infection. J Immunol 1992;148:2175–80.
24. Kallen KJ. The role of transsignalling via the agonistic soluble IL-6 receptor in human diseaes. Biochim Biophys Acta 2002;1592:323–43.
25. Jones SA, Rose-John S. The role of soluble receptors in cytokine biology: the agonistic properties of the sIL-6. R/IL-6 complex. Biochim Biophys Acta 2002;1592:251–63.
26. Horiuchi S, Ampofo W, Koyanagi Y, Yamashita A, Waki M, Matsumoto A, Yamamoto M, Yamamoto N. High-level production of alternatively spliced soluble interleukin-6 receptor in serum of patients with adult T-cell leukaemia/HTLV-I-associated myelopathy. Immunology 1998;95:360–9.
27. Yoshida T, Miyagawa E, Yamaguchi K, Kobayashi S, Takahashi Y, Yamashita A, Miura H, Itoyama Y, Yamamoto N. IL-2 independent transformation of unique human T cell line, TY-8–3 and its subclones by HTLV-I and -II. Int J Cancer 2001;91:99–108.
28. Kannagi M, Kuroda M, Maeda Y, Harada S. Coexistence of fusion receptors for human T-cell leukemia virus type-I (HTLV-I) and human immunodeficiency virus type-I (HIV-1) on MOLT-4 cells. Microbiol Immunol 1991;35:729–40.
29. Ohtani K, Nakamura M, Saito S, Nagata K, Sugamura K, Hinuma Y. Electroporation: application to human lymphoid cell lines for stable introduction of a transactivator gene of human T-cell leukemia virus type 1. Nucl Acids Res 1989;17:1589–604.
30. Ohtani K, Tsujimoto A, Tsukahara T, Numata N, Miura S, Sugamura K, Nakamura N. Molecular mechanisms of promorter regulation of the gp34 gene that is trans-activated by an oncoprotein Tax of human T cell leukemia virus type I. J Biol Chem 1998;273:14119–29.
31. Horiuchi S, Koyanagi Y, Zhou Y, Miyamoto H, Tanaka Y, Waki M, Matsumoto A, Yamamoto M, Yamamoto N. Soluble interleukin-6 receptor released from T cell or granulocyte/macrophage cell lines and human peripheral blood mononuclear cells are generated through an alternative splicing mechanism. Eur J Immunol 1994;24:1945–8.
32. Kieran M, Blank V, Logeat F, Vandekerckhove J, Lottspeich F, Le Bail O, Urban MB, Kourilsky P, Beauerle PA, Israel A. The DNA binding subunit of NF-κB is identical to factor KBF1 and homologous to the rel oncogene product. Cell 1990;62:1007–18.
33. Yoshida M. HTLV-I oncoprotein Tax deregulates transcription of cellular genes through multiple mechanisms. J Cancer Res Clin Oncol 1995;121:521–8.
34. McGuire KL, Curtiss VE, Larson EL, Haseline WA. Influence of human T-cell leukemia virus type I tax and rex on interleukin-2 gene expression. J Virol 1993;67:1590–9.
35. Mariner JM, Lantz V, Waldmann TA, Azimi N. Human T cell lymphotropic virus type I Tax activates IL-15. R alpha gene expression through an NF-κB site. J Immunol 2001;166:2602–9.
36. Mori N, Shirakawa F, Shimizu H, Murakami S, Oda S, Yamamoto K, Eto S. Transcriptional regulation of the human interleukin-6 gene promoter in human T-cell leukemia virus type 1-infected T-cell lines: evidence for the involvement of NF-κB. Blood 1994;84:2904–11.
37. Jones SA, Horiuchi S, Novick D, Yamamoto N, Fuller GM. Shedding of the soluble IL-6 receptor is triggered by Ca^{2+} mobilization, while basal release is predominantly the product of differential mRNA splicing in THP-1 cells. Eur J Immunol 1998;28:3514–22.
38. Jones SA, Novick D, Horiuchi S, Topley N, Yamamoto N, Szalai AJ, Fuller GM. C-reactive protein: a physiological activator of interleukin 6 receptor shedding. J Exp Med 1999;189:599–604.
39. Nowell MA, Richards PJ, Horiuchi S, Yamamoto N, Rose-John S, Topley N, Williams AS, Jones AS. Soluble IL-6 receptor governs IL-6 activity in experimental arthritis: blockade of arthritis severity by soluble glycoprotein 130. J Immunol 2003;171:3202–9.
40. Takemoto S, Mulloy JC, Cereseto A, Migone TS, Patel BK, Matsuoka M, Yamaguchi K, Takatsuki K, Kamihira S, White JD, Leonard WJ, Waldmann T, et al. Proliferation of adult T cell leukemia/lymphoma cells is associated with the constitutive activation of JAK/STAT proteins. Proc Natl Acad Sci USA 1997;94:13897–902.
41. Darnell JE, Jr, Kerr IM, Stark GR. Jak-STAT pathways and transcriptional activation in response to IFNs and other extracellular signaling proteins. Science 1994;264:1415–21.
42. Uchiyama T. Human T cell leukemia virus type I (HTLV-I) and human diseases. Annu Rev Immunol 1997;15:15–37.
43. Nagai M, Usuku K, Matsumoto W, Kodama D, Takenouchi N, Moritoyo T, Hashiguchi S, Ichinose M, Bangham CRM, Izumo S, Osame M. Analysis of HTLV-I proviral load in 202 HAM/TSP patients and 243 asymptomatic HTLV-I carriers: high proviral load strongly predisposes to HAM/TSP. J Neurovirol 1998;4:586–93.
44. Bowman T, Garcia R, Turkson J, Jove R. STATs in oncogenesis. Oncogene 2000;19:2474–88.
45. Migone TS, Lin JX, Cereseto A, Mulloy JC, Oshea JJ, Franchini G, Leonard WJ. Constitutively activated Jak-Stat pathway in T cells transformed with HTLV-I. Science 1995;269:79–81.
46. Nakamura N, Fujii M, Tsukahara T, Arai M, Ohashi T, Wakao H, Kannagi M, Yamamoto N. Human T-cell leukemia virus type 1 Tax protein induces the expression of STAT1 and STAT5 genes in T-cells. Oncogene 1999;18:2667–75.
47. Zhang Q, Lee B, Korecka M, Li G, Weyland C, Eck S, Gessain A, Arima N, Lessin SR, Shaw LM, Luger S, Kamoun M, et al. Differences in phosphorylation of the IL-2R associated JAK/STAT proteins between HTLV-I (+), IL-2-independent and IL-2-dependent cell lines and uncultured leukemic cells from patients with adult T-cell lymphoma/leukemia. Leuk Res 1999;23:373–84.
48. Umehara F, Izumo S, Takeya M, Takahashi K, Sato E, Osame MM. Expression of adhesion molecules and monocyte chemoattractant protein-1 (MCP-1) in the spinal cord lesions in HTLV-I-associated myelopathy. Acta neuropathol (Berl) 1996;91:343–50.
49. Arai M, Ohashi T, Tsukahara T, Murakami T, Hori T, Uchiyama T, Yamamoto N, Kannagi M, Fujii M. Human T-cell leukemia virus type I tax protein induces the expression of lymphocyte chemoattractant SDF-1/PBSF. Virology 1998;241:298–303.
50. Mihara M, Moriya Y, Kishimoto T, Ohsugi Y. Interleukin-6 (IL-6) induces the proliferation of synovial fibroblastic cells in the presence of soluble IL-6 receptor. Br J Rheumatol 1995;34:321–5.
51. Modur V, Li Y, Zimmerman GA, Prescott SM, Mcintyre TM. Retrograde inflammatory signaling from neutrophils to endothelial cells by soluble interleukin-6 receptor alpha. J Clin Invest 1997;100:2752–6.
52. Romano M, Sironi M, Toniatti C, Polentarutti N, Fruscella P, Ghezzi P, Faggioni R, Luini W, Van Hinsbergh V, Sozzani S, Bussolino F, Poli V, et al. Role of IL-6 and its soluble receptor in induction of chemokines and leukocyte recruitment. Immunity 1997;6:315–25.
53. McLoughlin RM, Witowski J, Robson RL, Wilkinson TS, Hurst SM, Williams AS, Williams JD, Rose-John S, Jones SA, Topley N. Interplay between IFN-gamma and IL-6 signaling governs neutrophil trafficking and apoptosis during acute inflammation. J Clin Invest 2003;112:598–607.
54. Teague TK, Marrack P, Kappler JW, Vella AT. IL-6 rescues resting mouse T cells from apoptosis. J Immunol 1997;158:5791–6.
55. Atreya R, Mudter J, Finotto S, Mullberg J, Jostocjk T, Wirwtz S, Schutz M, Bartsch B, Holtmann M, Becker C, Strand D, Czaja J, et al. Blockade of interleukin 6 trans signaling suppresses T-cell resistance against apoptosis in chronic intestinal inflammation: evidence in Crohn disease and experimental colitis in vivo. Nat Med 2000;6:583–8.
56. Teague TK, Schaefer BC, Hildeman D, Bender J, Mitchell T, Kappler JW, Marrack P. Activation-induced inhibition of interleukin 6-mediated T cell survival and signal transducer and activator of transcription 1 signalling. J Exp Med 2000;191:915–25.

Virus Genes (2006) 32:105–113
DOI 10.1007/s11262-005-5851-2

ORIGINAL ARTICLE

Analysis of human immunodeficiency virus type 1 integration by using a specific, sensitive and quantitative assay based on real-time polymerase chain reaction

Norio Yamamoto · Chika Tanaka · YuFeng Wu · Myint Oo Chang · Yoshio Inagaki · Yasunori Saito · Toshio Naito · Hitoshi Ogasawara · Iwao Sekigawa · Yasuo Hayashida

Received: 28 June 2005 / Accepted: 7 July 2005

Abstract A novel real-time nested-PCR assay was developed to quantify integrated human immunodeficiency virus type-1 (HIV-1) DNA with high specificity and sensitivity. This assay reproducibly allowed the detection of three copies of integrated HIV DNA in a background of 100,000 cell equivalents of human chromosomal DNA. The non-specific amplification of unintegrated HIV-1 DNA was significantly inhibited in this assay and the specificity of this assay was much higher than the previously reported method. This assay showed that kinetics in viral DNA sysnthesis was cell type dependent and that the kinetics of HIV-1 DNA integration was very rapid in Jurkat T cell line. This method may provide new insights into the integration processes and be useful in evaluating future integrase inhibitors.

Keywords HIV-1 · Integration · *Alu*-PCR · Real-time PCR · Nested PCR

N. Yamamoto (✉) · YuFeng Wu · M. O. Chang · Y. Inagaki · Y. Saito
Department of Molecular Virology,
1-5-45 Yushima, 113-8519,
Bunkyo-ku, Tokyo, Japan
e-mail: norio.mmb@tmd.ac.jp

C. Tanaka · T. Naito · Y. Hayashida
Department of General Medicine,
Juntendo University School of Medicine,
2-1-1 Hongo, 113-8421,
Bunkyo-ku,
Tokyo, Japan

H. Ogasawara
Department of Internal Medicine and Rheumatology,
Juntendo University School of Medicine,
2-1-1 Hongo, 113-8421,
Bunkyo-ku,
Tokyo, Japan

I. Sekigawa
Institute for Environmental and Gender Specific Medicine,
Juntendo University Graduate School of Medicine,
2-1-1 Tomioka, 279-0021,
Urayasu-shi,
Chiba, Japan

Introduction

Integration of viral DNA into the host cell genome is common to all retroviruses and is indispensable for a productive human immunodeficiency virus type 1 (HIV-1) infection [1–4]. The RNA genome of HIV-1 is reversely transcribed into double-stranded linear DNA in the cytoplasm. The resulting linear DNA molecule is actively transported to the nucleus as a component of the preintegration complex, which is the immediate precursor for the integration reaction [5–9]. In addition, HIV-1 DNA circles with one or two long terminal repeats (LTRs) are also transported to the nucleus [10, 11].

In contrast to investigations on the unintegrated forms of HIV-1 DNA, quantitative analysis of integrated HIV DNA has been hampered by the lack of an appropriate assay. To distinguish between extrachromosomal and integrated HIV-1 DNA, several assays have been developed including *Alu*-HIV PCR, where a pair of primers anneal to the HIV-1 sequence and the highly repeated chromosomal *Alu* elements [12, 13]. However, previous *Alu*-HIV PCR methods have limited specificity due to the non-specific amplification of unintegrated HIV-1 DNA.

To accurately quantify integrated HIV-1 DNA with high specificity and sensitivity, we have developed a new method based on real-time nested *Alu*-HIV PCR. Using this method we analyzed viral DNA integration in several kinds of cells. In addition to the study of HIV-1 DNA integration, real-time PCR was used to monitor the copy number of total HIV-1 DNA and 2LTR circles during a single-round of viral replication.

Materials and methods

Cells, plasmids, and viruses

Peripheral blood mononuclear cells (PBMCs) were isolated with Ficoll-Paque PLUS (Amersham Biosciences AB, Uppsala, Sweden). Cells were washed twice with phosphate-buffered saline (PBS) and resuspended in RPMI 1640 with 10% fetal calf serum (FCS), 100 IU/ml of penicillin and 100 μg/ml of streptomycin. PBMCs were stimulated with 5 μg/ml of phytohemoagglutinin (PHA) and 100 U/ml of IL-2 or cultured without any stimulation. Jurkat cells, U937 cells and 293T cells were maintained in RPMI 1640 supplemented with 10% FCS and antibiotics.

The pNL-bsr delta env vector and the pNLE delta env vector were constructed by deleting the envelope-coding sequence of the NL4-3 genome and replacing a nef-coding sequence with a blasticidin resistance gene and EGFP gene, respectively. Virus stocks were prepared by cotransfection of 293T cells with a HIV-1-encoding plasmid and VSV-G expression vector.

Infection of cells with pseudotyped HIV-1

The virus stocks were treated with DNase-I to remove residual plasmid DNA. Cells were infected with VSV-G-pseudotyped NLE-delta env virus where the amount of p24 gag antigen was 30 ng per million cells. One hour after infection, the cells were washed three times with phosphate-buffered saline (PBS) and cultured in RPMI 1640 supplemented with 10% fetal calf serum. At each time point, one million cells were lysed with buffer for DNA extraction.

Generation of an integrated HIV-1 DNA standard

In order to precisely determine the copy number of integrated HIV-1 DNA, the standard cells should contain numerous randomized integration sites with a wide distribution of distances between the provirus and the nearest *Alu* sequences. To generate an appropriate HIV-1 DNA standard for quantification of integrated viral DNA, Jurkat cells were infected with NL-bsr delta env virus pseudotyped with VSV-G. Infected Jurkat cells were then cultured in the presence of blasticidin (10 μg/ml) to select cells which carried integrated viral DNA. Five days after initiation of the blasticidin selection, the number of resistant cells was counted. A total of one million cells were blasticidin-resistant, and the number of independent clones was estimated at more than 30,000. In our standard cell line, named Jurkat/NL-bsr, the copy number of integrated viral DNA is equal to the total HIV-1 DNA copy number because unintegrated forms of HIV-1 DNA were lost during the numerous rounds of cell division. Thus, based on total HIV-1 DNA and beta-globin quantifications, we estimated that, Jurkat/NL-bsr contained 5.44±0.05 proviruses per cell.

Real-time nested *Alu*-HIV PCR assay procedures

Real-time nested PCR was performed using an ABI-7700 sequence detector system (Applied Biosystems). During the first-round PCR, integrated HIV-1 sequences were amplified with the HIV-1 gag-specific primer (first-gag-R) and *Alu*-targeting primers (first-*Alu*-F and first-*Alu*-R) that annealed to conserved regions of the *Alu* repeat element (Fig. 1a). During the first-round PCR, *Alu*-gag sequences were amplified from 1/10 of total cell DNA in a 25 μl reaction mixture comprising 1×Taqman buffer A, 3.5 mM $MgCl_2$, 200 μM dNTP, 300 nM primers, 200 nM probe, and 0.025 U/μl AmpliTaq Gold. The first-round PCR cycle conditions were as follows: a DNA denaturation and polymerase activation step of 10 min at 95°C and then 12 cycles of amplification (95°C for 15 s, 60°C for 30 s, 72°C for 5 min). Due to the presence of numerous *Alu* elements within the human genome (at least 900,000 copies per haploid genome, giving an average distance of 4 kb between *Alu* elements [14]), abundant amplification of inter-*Alu* sequences occurred simultaneously with the amplification of *Alu*-HIV sequences. Only 12 cycles of amplification were performed to keep the reaction in the exponential phase.

During the second-round PCR, the first-round PCR product could be specifically amplified by using the tag-specific primer (second-tag-R) and the LTR primer (second-LTR-F) (Fig. 1b). The second-round PCR was performed on 1/25 of the first-round PCR product in a mixture comprising 1× Taqman buffer A, 3.5 mM $MgCl_2$, 200 μM dNTP, 300 nM primers, 600 nM probe, and 0.025 U/μl AmpliTaq Gold. The second-round PCR cycles began with a DNA-denaturation and polymerase-activation step (95°C for 10 min), followed by 45 cycles of amplification (95°C for 15 s, 60°C for 60 s).

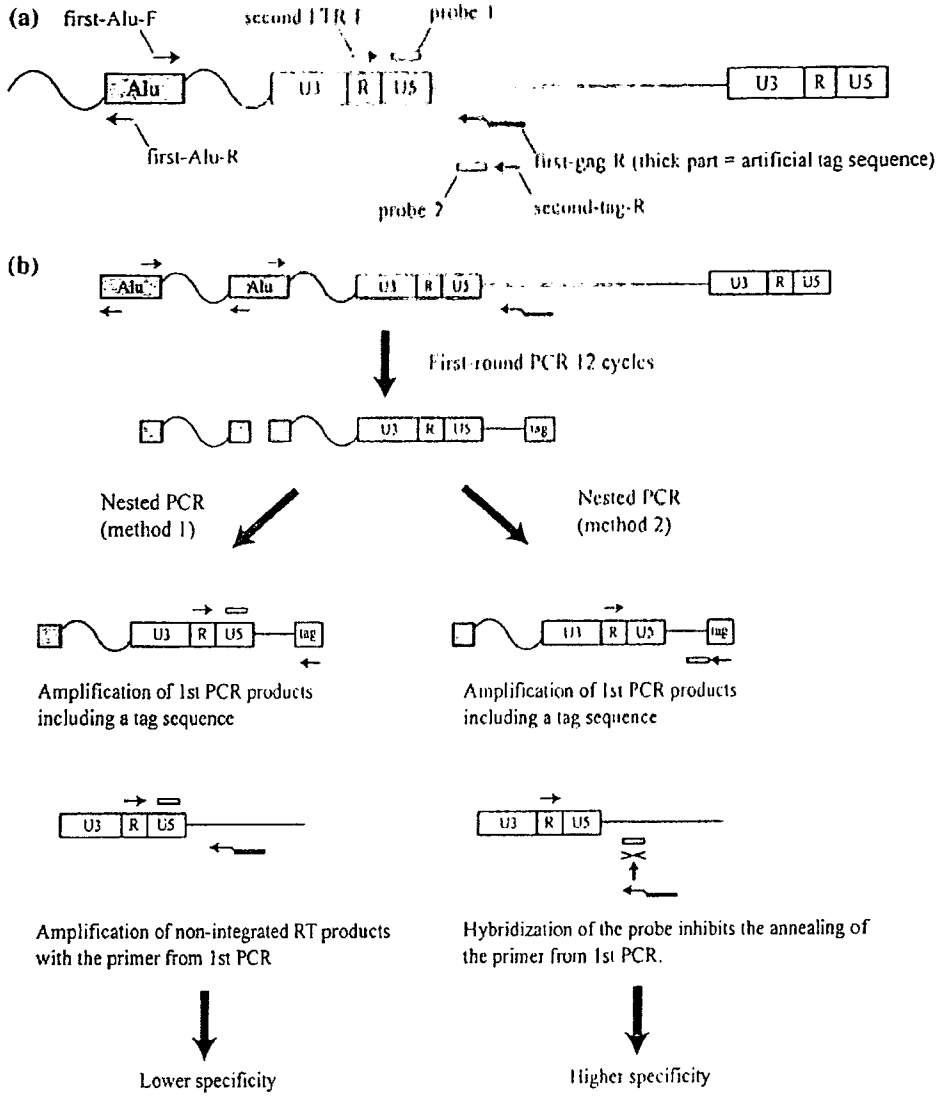

Fig. 1 Strategies for real-time nested PCR. (a) Location of primers and probes for the quantification of integrated HIV-1 DNA. (b) Comparison of two strategies to quantify integrated HIV-1 DNA

Real-time PCR assay for quantification of total viral DNA and 2LTR DNA

The total HIV-1 DNA copy number was determined with the primers that annealed in the U5 region of the LTR (total-F) and in the 5′ end of the gag gene (total-R) (Table 1). The 2LTR circles were amplified with primers spanning the LTR–LTR junction (circle-F and circle-R) (Table 1). The sequences of U5-gag and two-LTR junctions were amplified from 1/50 of total cell DNA according to the manufacturer's instructions. The copy numbers of total HIV-DNA and 2LTR circles were determined in reference to a standard curve prepared by amplification of quantities ranging from 10 to 100,000 copies of cloned DNA with matching sequences. The cell equivalents in sample DNA were calculated based on the amplification of the beta-globin gene (two copies per diploid cell) with ABI-7700 sequence detector system. The results of quantification were expressed as copy numbers per 1000 cells.

Results

Strategy of the previous real-time nested PCR and a novel real-time nested PCR

During the first-round PCR, integrated HIV-1 sequences were amplified with the HIV-1 gag-specific primer and

Table 1 Primer and probe sequences

Primer or probe	Sequence (5′-3′)	Target
first-*Alu*-F	AGCCTCCCGAGTAGCTGGGA	Integrated HIV-1 DNA (first-round PCR)
first-*Alu*-R	TTACAGGCATGAGCCACCG	
first-gag-R	CAATATCATACGCCGAGAGTGCGCGCTTCAGCAAG	
second-LTR-F	TTGTTACACCCTATGAGCCAGC	Integrated HIV-1 DNA (second-round PCR)
second-tag-R	CAATATCATACGCCGAGAGTGC	
probe-1	AGTGTGTGCCCGTCTGTTGTGTGACTC*	
probe-2	CGCTTCAGCAAGCCGAGTCCTGC*	
total-F	CCGTCTGTTGTGTGACTCTGG	Total HIV-1 DNA
total-R	GAGTCCTGCGTCGAGAGATCT	
total-probe	TCTAGCAGTGGCGCCCGAACAGG*	
circle-F	CCCTCAGACCCTTTTAGTCAGTG	2LTR circle DNA
circle-R	TGGTGTGTAGTTCTGCCAATCA	
circle-probe	TGTGGATCTACCACACACAAGGCTACTTCC*	

*Modified with FAM at the 5′ end and with TAMRA at the 3′ end. The tag sequence in the first-gag-R primer is underlined

Alu-targeting primers that annealed to conserved regions of the *Alu* repeat element (Fig. 1a). Since *Alu* elements are present in either orientation relative to the integrated provirus, the use of two outward-facing *Alu* primers optimized the amplification of *Alu*-gag sequences integrated into the host cell genome (Fig. 1a). To decrease amplification of nonintegrated reverse transcription products, we used an HIV-1 gag-specific primer extended with an artificial tag sequence at the 5′ end of the oligonucleotide (first-gag-R) in the first round of amplification and the primer which matches this artificial sequence (second-tag-R) in the second-round PCR (Fig. 1b).

The method 1 shown in Fig. 1b is equivalent to previously established real-time nested PCR assay and the method 2 is a novel assay developed by us. In the second-round PCR using the tag-specific primer and the LTR primer, the first-round PCR product could be amplified with lower background by the method 1. However, unintegrated viral DNA could be amplified in the method 1 even when the tag-specific primer was used for amplification. Because one twenty fifth of the reaction mixture after 12 cycles of the first-round PCR was used as a template for the second-round PCR, unintegrated reverse transcription products could be amplified with the forward primer for second-round PCR (second-LTR-F) and the residual reverse primer for first-round PCR (first-gag-R) (Fig. 1b). To prevent non-specific amplification of unintegrated reverse transcription products, we designed a new method (method 2) using probe-2 which has a sequence overlapping the first-gag-R primer. Probe-2 can preferentially hybridize to the target sequence and inhibit hybridization of the residual first-gag-R primer during the second-round PCR, because the melting temperature of probe-2 is much higher than that of the first-gag-R primer (Fig. 1b).

Specificity of the novel real-time nested PCR assay.

To assess the extent of non-specific amplification of unintegrated reverse transcription products in method 1 and method 2, we compared the fluorescence curves generated during the second-round PCR after three different first-round reactions: (1) in the presence of 3 primers (first-*alu*-F, first-*alu*-R, first-gag-R) with polymerase (primer+ / polymerase+), (2) in the presence of 3 primers without polymerase (primer+/polymerase−), and (3) in the absence of 3 primers without polymerase (primer−/ polymerase−). The fluorescence curve of primer+/polymerase+in the method 1 significantly shifted to the left in comparison to that of the primer−/polymerase−reaction (Fig. 2a). However, the fluorescence curve of primer+/polymerase−in the method 1 shifted as much as that of primer+/polymerase+ (Fig. 2a). This means that the extent of amplification of unintegrated reverse transcription products with the second-LTR-F primer and the first-gag-R primer was considerable. Probe-2, which was used in the method 2, preferentially hybridized to the target sequence and inhibited hybridization of the first-gag-R primer during the second-round PCR, because the melting temperature of probe-2 is much higher than that of the first-gag-R primer (Fig. 1b). As shown in Figure 2b, the fluorescence curve of primer+/ polymerase− in the method 2 shifted to the right dramatically compared with the curve of primer+/polymerise-in the method 1. The shift by using probe-2 instead of probe-1 was about 4 log10 units (17 cycles), which indicated that the specificity of the method 2 was much higher than that of the method 1.

Sensitivity of the novel real-time nested PCR assay.

The copy number of integrated HIV-1 DNA was determined in reference to a standard curve given by an array of serially

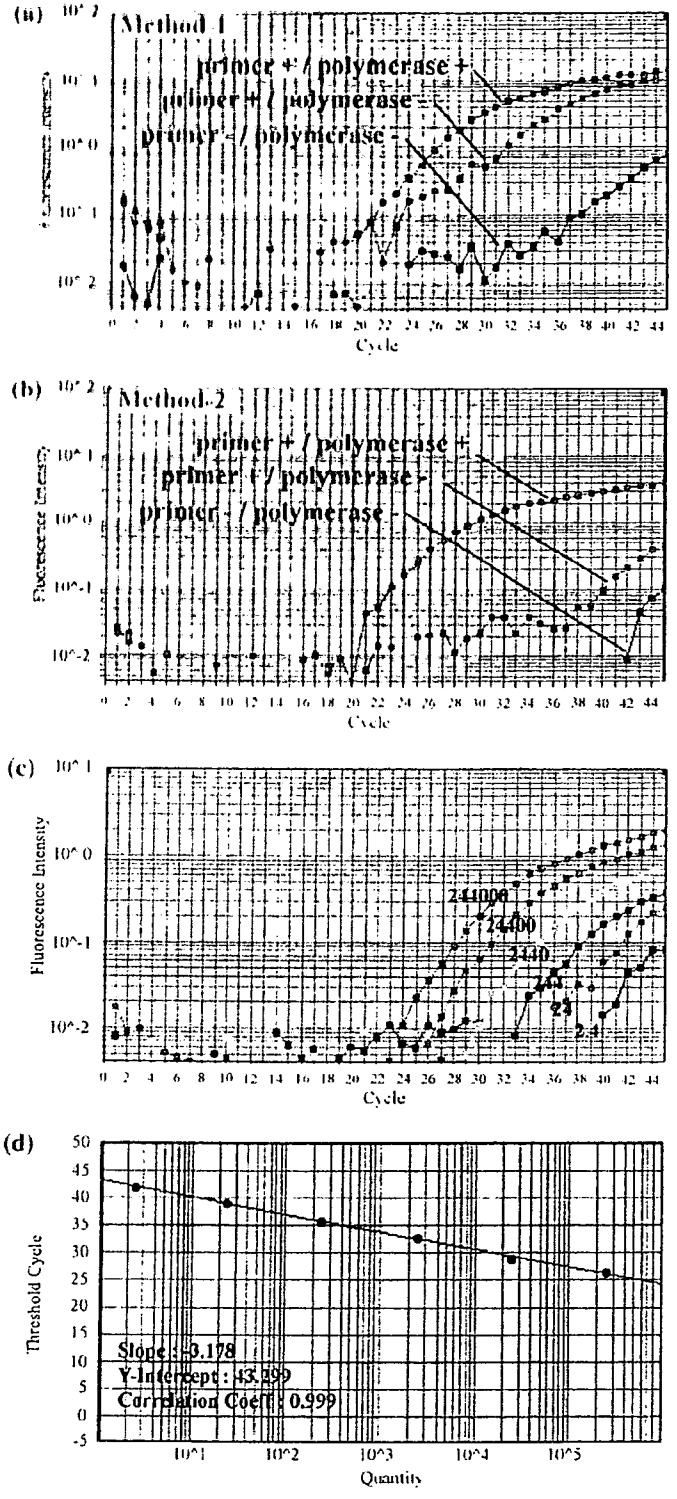

Fig. 2 Characteristics of real-time nested PCR. (**a** and **b**) Fluorescence curves generated by amplification of provirus DNA from HL60 cells infected with VSV-G-pseudotyped NLE delta env virus. (**a**) Fluorescence curves of probe-1 used in method 1. (**b**) Fluorescence Curves of probe-2 used in method 2. (**c**) Fluorescence curves generated by two-step amplification of serial dilutions of Jurkat/NL-bsr cell DNA. The copy numbers for each standard DNA are shown on the corresponding fluorescence curve. (**d**) Linear regression to quantify integrated HIV-1 DNA

diluted Jurkat/NL-bsr cell DNA mixed with uninfected Jurkat cell DNA to yield 100,000 cell equivalents. In our system, the regression obtained from amplification of serial dilutions of the integrated HIV-1 DNA was linear over a 6-log 10-unit range, and this *Alu*-HIV nested PCR allowed the detection of approximately three proviruses in 100,000 cell equivalents (Fig. 2c and 2d). The sensitivity of our system is as high as that of previously reported methods [15–18].

Analysis of early HIV-1 DNA synthesis in Jurkat cells infected with VSV-G-pseudotyped virus

To assess the time point when integration of HIV-1 takes place, we quantified integrated HIV-1 DNA in a single round of viral replication with the novel real-time nested PCR assay.

Total HIV-1 DNA was detected 3 h post infection and reached a maximum of 7,726 copies per 1000 cells at 5 h post infection (Fig. 3a). Subsequently a steep decrease phase and a slow decrease phase were observed. This novel real-time nested PCR assay detected integrated HIV-1 DNA within 3 h of infection, which indicated that reverse transcription products were imported to the nucleus immediately and integrated into the host cell genome very rapidly (Fig. 3b). The copy number of integrated proviruses reached a maximum of 1398 copies per 1000 cells at 5 h post infection and remained at the same level after this time point, which suggested that HIV-1 integration was completed by 5 h post infection in Jurkat cells (Fig. 3b). Two-LTR circles were detected by 3 h post infection but the copy number of 2LTR circles was not as high as that of integrated HIV-1 DNA. (Fig. 3c).

Comparison of viral DNA synthesis in Jurkat cells, U937 cells, resting PBMCs and activated PBMCs

We compared the kinetics of viral DNA synthesis in several kinds of cells to elucidate the relationship between viral DNA synthesis and status of cells (Fig. 4). Jurkat cells, U937 cells, unstimulated PBMCs and PHA/IL-2-activated PBMCs were infected with VSV-G pseudotyped HIV-1 and these cells were lysed with DNA extraction buffer at 3 h, 6 h, 12 h, 24 h and 48 h post infection. Time points of sample collection were determined based on the result of detailed kinetic analysis in Jurkat cells (Fig. 3).

Efficiency of reverse transcription was quite different in each type of cells. Jurkat cells and U937 cells were highly active in reverse transcription (Fig. 4a) and activated PBMCs were moderately active (Fig. 4b). In resting PBMCs reverse transcription efficiency was very low (Fig. 4b). Two cell lines with higher reverse transcription activity, Jurkat cells and U937 cells, exhibited three phases in the kinetics of total DNA: a rapid rising phase, a steep falling phase and a slow falling phase (Fig. 4a). Activated and resting PBMCs, which showed lower reverse transcription efficiency, exhibited only a slow rising phase (Fig. 4b).

The kinetics of viral DNA integration was also dependent on the cells. Integration of viral DNA in Jurkat cells and U937 cells was completed by 12 h post infection (Fig. 4c, d). Activated PBMCs showed complete integration in 24 h (Fig. 4d). The cope number of proviral DNA in resting PBMCs reached a maximum level at 48 h (Fig. 4d). Efficiency of 2LTR circle formation was different in each cell type. Synthesis of two LTR circles reached its peak at the same time point when viral DNA integration reached its maximum level (Fig. 4e, f). Ratio of 2LTR DNA to proviral DNA was low in all cells (0.1–0.6%)

Discussion

We could have developed a novel assay with high specificity and sensitivity to quantify integrated viral DNA of HIV-1. Our study showed that specificity of this nested PCR assay is much higher than that of the previously reported methods [15–19].

We could find four previous methods to quantify integrated viral DNA: (1) methods based on one-step amplification, (2) methods based on nested PCR using linker-primer (nested LP-PCR), (3) methods based on real-time nested PCR using *Alu*-specific primers and a virus-specific primer without tag sequence, (4) methods based on real-time nested PCR using *Alu*-specific primers and a virus-specific primer with tag sequence.

The novel real-time nested PCR assay detected integrated HIV-1 DNA as early as 3 h after infection while the one-step amplification method allowed the detection of proviral DNA later than 12 h [20] or 24 h [19] after infection. The delayed detection of integrated HIV-1 DNA in the one-step real-time PCR might be due to the limited sensitivity of this assay.

Other methods based on nested LP-PCR had been devised [15, 16]. The protocol of the nested LP-PCR involved many experimental steps, one of which is amplification of LTR in the second-round PCR. The nested LP-PCR amplified the LTR sequence and did not prevent the amplification of unintegrated forms of HIV-1 because of the absence of a tag sequence in the primer.

Recently, a real time nested PCR method with the *Alu* element-specific primers and HIV-1 gag-specific primer without tag sequence was described, in which the LTR sequence was amplified during the second-round PCR [17]. This real-time nested PCR did not prevent the amplification of unintegrated forms of HIV-1 due to the lack of tag sequence in the primer.

More recently, Brussel et al. [18] developed a new real-time nested PCR using an extended LTR primer with a tag sequence for the first-round PCR and the tag-specific primer for the second-round PCR to amplify only products from the first-round PCR. However, even this well-devised method could not prevent the residual tagged primer used in first-round PCR from annealing to the unintegrated forms of HIV-1 DNA, which resulted in lower specificity

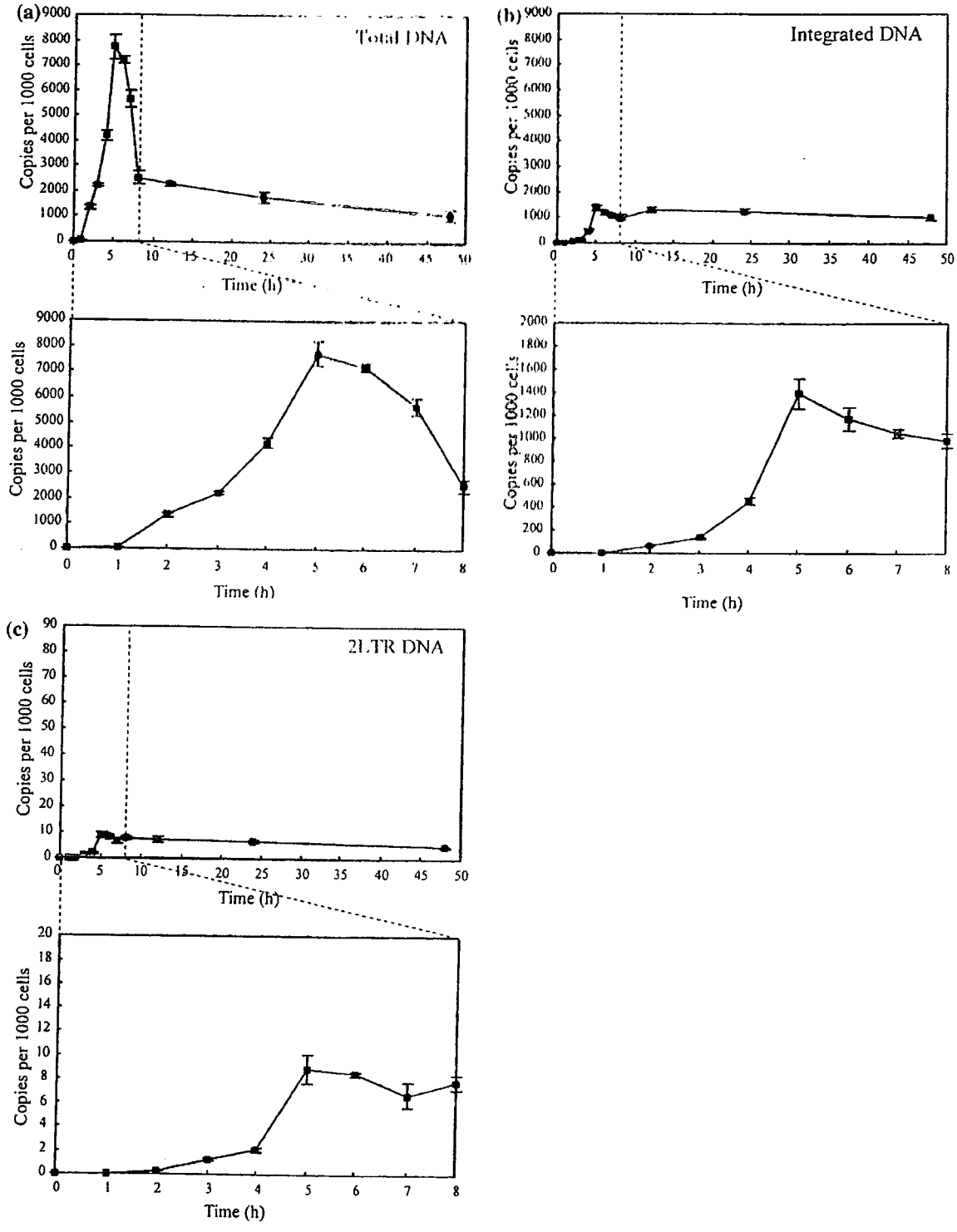

Fig. 3 Detailed quantification of HIV-1 DNA during a single round infection of Jurkat cells with VSV-G-pseudotyped NL-E delta env virus. (a) Time course analysis of total HIV-1 DNA, (b) integrated HIV-1 DNA and (c) 2LTR circle DNA. Values are shown as means±standard errors

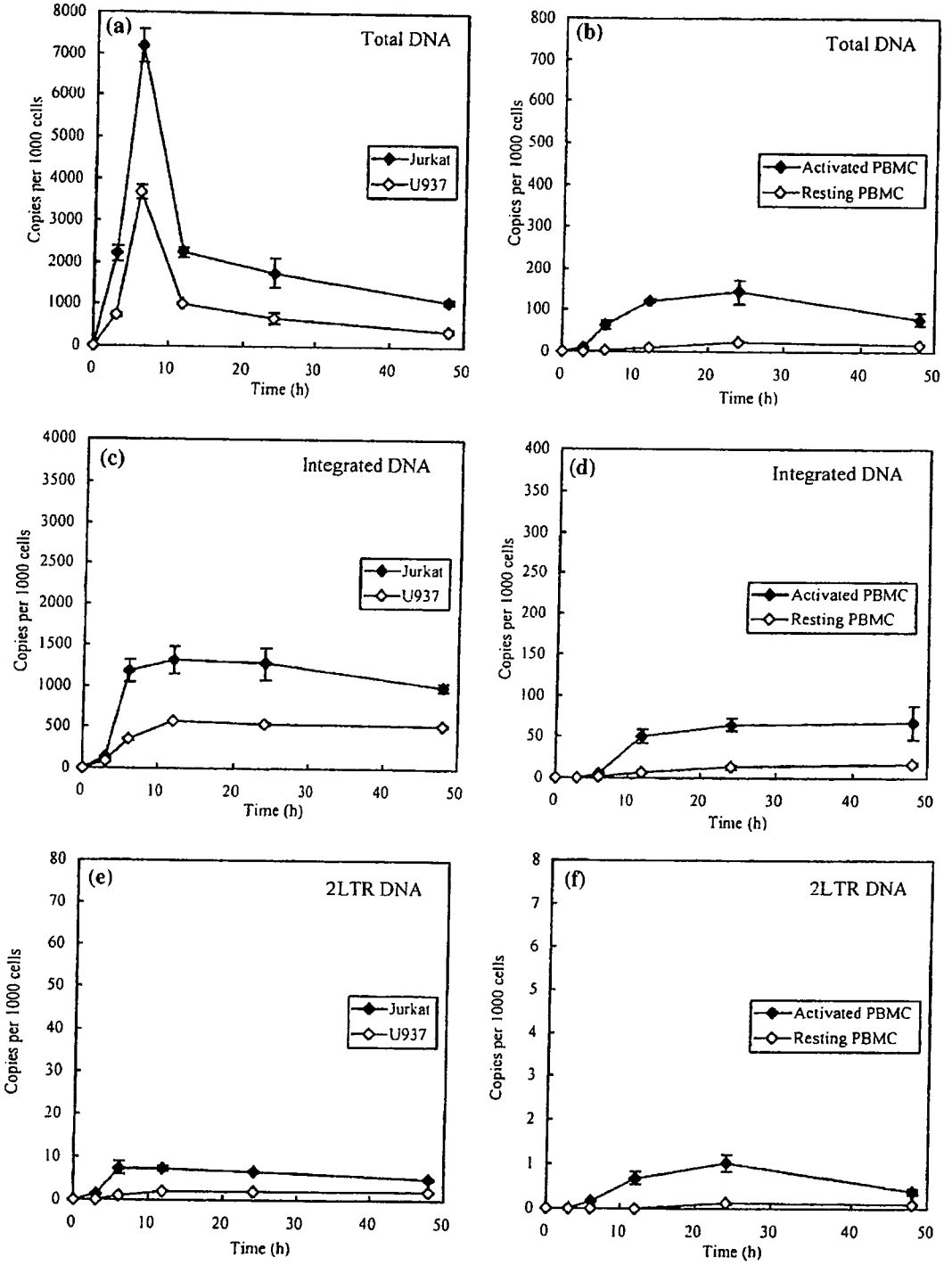

Fig. 4 Quantification of HIV-1 DNA synthesis during a single round infection of Jurkat cells, U937 cells, PHA/IL-2 activated PBMCs and resting PBMCs with VSV-G-pseudotyped NL-E delta env virus. (**a**) Time course analysis of total HIV-1 DNA synthesis in Jurkat cells and U937 cells, and (**b**) in PHA/IL-2 activated PBMCs and resting PBMCs. (**c**) Time course analysis of HIV-1 DNA integration in Jurkat cells and U937 cells, and (**d**) in PHA/IL-2 activated PBMCs and resting PBMCs. (**e**) Time course analysis of 2LTR DNA formation in Jurkat cells and U937 cells, and (**f**) in PHA/IL 2 activated PBMCs and resting PBMCs. Values are shown as means±standard errors